**Rational design and experimental evaluation of peptide ligands for the purification of adeno-associated viruses via affinity chromatography**

Shriarjun Shastry[1,2,§], Wenning Chu[1,§], Eduardo Barbieri[1], Paul Greback-Clarke[2], William K. Smith[2], Christopher Cummings[2], Arianna Minzoni[1], Jennifer Pancorbo[2], Gary Gilleskie[2,*], Kimberly Ritola[3,4], Michael A. Daniele[4,5,*], and Stefano Menegatti[1,2,4,6,*]

[1] Department of Chemical and Biomolecular Engineering, North Carolina State University, 911 Partners Way, Raleigh, NC 27606, USA

[2] Biomanufacturing Training and Education Center (BTEC), North Carolina State University, 850 Oval Dr, Raleigh, NC 27606, USA

[3] Neuroscience Center, Brain Initiative Neurotools Vector Core, University of North Carolina at Chapel Hill, 116 Manning Drive, Chapel Hill, NC 27599

[4] North Carolina Viral Vector Initiative in Research and Learning (NC-VVIRAL), North Carolina State University, 911 Oval Dr, Raleigh, NC 27695, USA

[5] Joint Department of Biomedical Engineering, North Carolina State University and University of North Carolina at Chapel Hill, 911 Oval Drive, Raleigh, NC 27695, USA

[6] LigaTrap Technologies LLC, Raleigh, NC 27606

[§] Indicates equal contributions.

[*] Corresponding authors: glgilles@ncsu.edu; mdaniel6@ncsu.edu; smenega@ncsu.edu.

**Abstract.** Adeno-associated viruses (AAVs) have acquired a central role in modern medicine as delivery agents for gene therapies targeting rare diseases. While new AAVs with improved tissue targeting, potency, and safety are being introduced, their biomanufacturing technology is lagging. The AAV purification pipeline, in particular, hinges on protein ligands for the affinity-based capture step: while featuring excellent AAV binding capacity and selectivity, these ligands require strong acid (pH <3) elution conditions, which can compromise the product's activity and stability; additionally, their high cost and limited lifetime has a significant impact on the price tag of AAV-based therapies. Seeking to introduce a more robust and affordable – yet equally effective – affinity technology, this study introduces a cohort of peptide ligands that *(i)* mimic the biorecognition activity of the AAV receptor (AAVR) and anti-AAV antibody A20, while *(ii)* enabling product elution under near-physiological conditions (pH 6.0) and *(iii)* granting extended reusability by withstanding multiple regenerations. A20-mimetic CYIHFSGYTNYNPSLKSC and AAVR-mimetic CVIDGSQSTDDDKIC demonstrated excellent capture of serotypes belonging to distinct clones/clades – AAV1, AAV2, AAV5, AAV6, AAV8, and AAV9 – corroborating the in silico models documenting their ability to target regions of the viral capsid that are conserved across all serotypes. CVIDGSQSTDDDKIC-Toyopearl resin features binding capacity (~$10^{14}$ vp per mL) and product yields (~60-80%) on par with commercial adsorbents, and purified AAV2 from HEK293 and Sf9 cell lysates affording high recovery (up to 78%) and reduction of host cell proteins (up to 700-fold), and high transduction activity (up to 65%) of the purified vectors.

**Keywords.** Gene therapy; adeno-associated virus; peptide ligands; affinity chromatography; transduction activity.

## 1. Introduction

Viral vectors are poised to become fundamental tools in modern medicine and biotechnology owing to their role as delivery agents of gene therapies targeting rare diseases, oncolytic agents to fight aggressive forms of cancer, vaccine platforms to counter infectious diseases, and a gateway to engineer plants and animals for a sustainable agriculture.[1-4] The landscape of viral vector technology is rich of promises as much as challenges: novel vector designs are constantly being introduced with improved tissue targeting and gene delivery activity as well as lower genotoxicity, hepatotoxicity, and immunogenicity.[5-7] At the same time, the bioprocess technology utilized in viral vector manufacturing draws heavily upon a decades-old platform established decades ago for producing monoclonal antibodies (mAbs). This is well exemplified by the purification pipeline of adeno-associated viruses (AAVs) – the vector of choice in gene therapy – where protein ligands that resemble the Protein A used for mAb purification are employed at the product capture step.[8,9]

The landscape of commercial affinity resins for AAV purification – now counting six adsorbents, including POROS™ CaptureSelect™ AAVX, AAV8 (CSAL8) and AAV9 (CSAL9), AVB Sepharose HP, Capto AVB, and AVIPure – uniformly relies on single-chain camelid antibody fragments derived from animal immunization or biological display libraries.[10,11] While providing the high binding strength and selectivity needed to isolate AAVs from current feedstocks, which typically feature low product titer and a wide abundance of impurities, these ligands also require the use of harsh aqueous buffers (pH $\leq$ 3) to release the bound capsids and limits the reusability of the resins, despite the high cost, due to their limited biochemical stability.[8,12]

Addressing the challenges stemming from the use of protein affinity ligands, our team has established a framework for discovering and developing peptide-based affinity ligands. Leveraging the chemical and structural diversity of peptides has delivered a collection of binders for protein purification that combine high selectivity and capacity with mild elution conditions: recent examples include ligands that release the product upon exposure to mild pH ($\geq$ 4),[13-16] kosmotropic salts ($MgCl_2$),[17] or light,[18,19] thus safeguarding the bioactivity of labile targets. The adoption of peptide ligands, which can be mass manufactured rapidly and affordably, is also conducive to reducing the production costs of viral vectors. This is particularly *à propos* in the field of gene therapy, where manufacturing costs – to which the purification segment contributes a great deal – result in staggering price tags to patients, ranging between $2.5-3.5M.[20]

Given the importance and growth of AAVs, amply documented by the surge in clinical trials and the uptick in regulatory approvals, we resolved to leverage our toolbox to develop AAV-targeting peptides. Relevant to our endeavor has been the wealth of data on AAV-targeting biomolecules – particularly the crystal structures of the complexes formed by AAVs of different serotypes with the AAV receptor (AAVR) and the anti-AAV antibody A20 – that has become available in the last decade. Accordingly, we undertook the rational design of cyclic peptide mimetics of AAVR and A20 by abstracting sequences that target regions of the capsids that are highly conserved across serotypes of different clades. At the same time, to overcome the limitations of protein ligands, the peptide mimetics were designed to form complexes with different AAV serotypes that *(i)* feature high-affinity at physiological conditions ($|\Delta G_b| \geq 6.5$ kcal/mol at pH 7.4) and *(ii)* undergo a $\geq$100-fold loss of binding strength as the pH is lowered to 6.5. Among the selected sequences, A20-mimetic CYIHFSGYTNYNPSLKSC and AAVR-mimetic CVIDGSQSTDDDKIC demonstrated excellent capture of serotypes belonging to distinct clones/clades – AAV1, AAV2, AAV5, AAV6, AAV8, and AAV9 – corroborating the *in silico* models documenting their ability to target regions of the virion proteins that are conserved across

all serotypes. CVIDGSQSTDDDKIC-Toyopearl resin features values of binding capacity (~$10^{14}$ vp per mL) and product yields (~60-80%) on par with commercial adsorbents, and purified AAV2 from a HEK293 cell lysate affording high recovery (70-80%), a 700-fold reduction of host cell proteins (HCPs), and high transduction activity (up to 65%) of the purified viruses.

## 2. Materials and Methods

***2.1. In silico design of peptide mimetics of the AAV receptor (AAVR) and anti-AAV antibody A20.*** The crystal structures of AAVR in complex with AAV1 (PDB ID: 6JCQ and 7TI5), AAV2 (3J1S, 6IHB and 6NZ0), AAV5 (7KP3 and 7KPN), and AAV9 (7WJX and 7WQP) as well as the complex of AAV2 with monoclonal antibody A20 (3J1S) were analyzed to identify the residues on the protein ligands (AAVR and A20) and the AAV virion protein (VP1) involved in the affinity interaction and calculate their pairwise contributions to the binding energy. Based on this analysis, the A20-mimetic candidates CYGHFSGYGNYGPC, CYGHFSPYGNYGPC, CYHFSYNYPC, CYHFSYNYPKSC, CYIHFSGYTNYNGSLKSC, CYIHFSGYTNYNPC, CYIHFSGYTNYNPSLKSC, CYIHFSPYTNYNPSLKSC, CYVHFSGYSNYSPSC, GCGQQYWIGPFTFGCG, GQQYWIGPFTFG, LETVKPGLYEPITHPRDYS, and SYDRPHTIPEYLGPKVTEL; and the AAVR-mimetic candidates AIVSPQFQEISLPTTSTVIDGSQSTDDDKIVQY, CDGSQSTDDDKIC, CDSQSTDDDKIC, CSGSTDDDKIC, CSGSTEQEKIC, CVIDGSQSTDDDKIC, CVIDGSQSTDDDKIVQYC, GCLITHPRDYS, GCLITHPRDYSGCG, GYIHFSGYTNYNPSLKS, GYWIGPFTGGGYIHFSGYT, GYWIGPFTGPGYIHFSGYT, GYWIGPFTPGPYIHFSGYT, LITHPRDYSPKLTPGLYEFG, and TVIDGSQSTDDDKIVQY were constructed using the molecular editor Avogadro[21] and their structures were prepared in GROMACS using the force field GROMOS 54A7;[22] disulfide-cyclic peptide sequences A1-A12 were designed in the cyclic format GC-$X_1X_2$[…]$X_n$-C-GSG, whereas linear peptide sequences A12-A16 were designed in the linear format G-$X_1X_2$[…]$X_n$-GSG. Each peptide sequence was placed in a simulation box with periodic boundary containing 1,500 TIP3P water molecules and equilibrated with 10,000 steps of steepest gradient descent; heated to 300 K in an NVT ensemble for 250 ps using 1 fs time steps; and equilibrated to 1 atm via a 500-ps NPT simulation with 2 fs time steps. The production runs were conducted in the NPT ensemble under constant 300 K and 1 atm by applying the Nosé-Hoover thermostat and the Parrinello-Rahman barostat, respectively;[23] the motion equations were integrated using the leap-frog algorithm with steps of 2 fs; covalent bonds were constrained using the LINCS algorithm; Lennard-Jones and short-range electrostatic interactions were calculated using cut-off values of 0.8 nm and 1.2 nm, respectively; the particle-mesh Ewald method was implemented for the long-range electrostatic interactions;[24-26] the lists of bonded and non-bonded interactions (cutoff of 1.2 nm) were updated every 2 and 6 fs, respectively. The energetic landscape associated to the various peptide conformations was sampled to identify the structures with absolute energy minima. The structure of the VP1 from AAV1 (PDB ID: 6JCR), AAV2 (6IH9), AAV3 (3KIC), AAV4 (2G8G), AAV5 (7KP3), AAV6 (5EGC), AAV7 (7JOT), AAV8 (2QA0), and AAV9 (7WJX) were initially prepared using Protein Prep Wizard (PPW, Schrödinger, New York, NY)[27] by correcting missing residues or atoms, adding explicit hydrogens, removing salt ions, and optimizing the hydrogen-bonding network. The resulting VPs were utilized to construct triangular clusters of VP1-VP2-VP3 proteins, whose ionization states at pH 6.0 and 7.4 were obtained - and the corresponding structural minimization of the clusters were performed using PROPKA.[28] The construct triangular clusters were finally draped on the spherical cap of the

corresponding AAV capsid. The peptide ligands were then docked *in silico* against the AAVR binding sites using the docking software HADDOCK (High Ambiguity Driven Protein-Protein Docking) v.2.4.[29,30] The AAVR-binding residues and the A20-binding residues on the VP proteins and residues $X_1X_2[\ldots]X_n$ on the peptides were denoted as "active", while all surrounding residues were marked as "passive". Clusters of up to 20 docked AAV:peptide structures selected based on Cα RMSD < 7.5 Å were ranked using the dMM-PBSA score.[31] Finally, the top AAV:peptide complexes were refined via 200-ns MD simulations to estimate the free energy of binding ($\Delta G_B$).

***2.2. Materials.*** Fluorenylmethoxycarbonyl- (Fmoc-) protected amino acids Fmoc-Ala-OH, Fmoc-Arg(Pbf)-OH, Fmoc-Asn(Trt)-OH, Fmoc-Asp(OtBu)-OH, Fmoc-Cys(Trt)-OH, Fmoc-Glu(OtBu)-OH, Fmoc-Gly-OH, Fmoc-His(Trt)-OH, Fmoc-Ile-OH, Fmoc-Leu-OH, Fmoc-Lys(Boc)-OH, Fmoc-Phe-OH, Fmoc-Pro-OH, Fmoc-Ser(tBu)-OH, Fmoc-Thr(tBu)-OH, Fmoc-Trp(Boc)-OH, Fmoc-Tyr(tBu)-OH, and Fmoc-Val-OH, the coupling agent Hexafluorophosphate Azabenzotriazole Tetramethyl Uronium (HATU), diisopropylethylamine (DIPEA), piperidine, and trifluoroacetic acid (TFA) were procured from ChemImpex International (Wood Dale, IL, USA). The Toyopearl NH2-750F resin (pore size > 100 nm; particle size: 45 µm; ligand density: 200 µmol per mL resin) was obtained from Tosoh Bioscience (Tokyo, Japan). Triisopropylsilane (TIPS), Kaiser test kits, 1,2-ethanedithiol (EDT), polybrene, and phosphate buffered saline (PBS) tablets were from MilliporeSigma (St. Louis, MO, USA). Dichloromethane (DCM), methanol, N-methyl-2-pyrrolidone (NMP), N,N'-dimethylformamide (DMF), Bis-Tris HCl, magnesium chloride ($MgCl_2$), phosphoric acid, potassium chloride (KCl), sodium chloride (NaCl), sodium hydroxide (NaOH), Pluronic™ F-68, POROS™ CaptureSelect™ AAVX Affinity Resin, and SilverQuest™ Silver Staining Kit were obtained from Fisher Chemical (Hampton, NH, USA). The AVB Sepharose HP was sourced from Cytiva (Marlborough, MA). Dulbecco's Modified Eagle Medium (DMEM) and fetal bovine serum (FBS), Gibco™ Viral Production Cells 2.0, AAV-MAX Enhancer, Viral-Plex™ Complexation Buffer, Transfection Reagent, benzonase endonuclease, and AAV-MAX Lysis Buffer were obtained from ThermoFisher Scientific (Waltham, MA). Human fibrosarcoma (HT1080) cells were sourced from ATCC (Manassas, VA). Pure AAV2, AAV6, AAV8, and AAV9 were sourced from Charles River Laboratories (Durham, NC). The Alltech chromatography columns (diameter: 3.6 mm; length: 50 mm; volume: 0.5 mL), and 10 µm polyethylene frits were obtained from VWR International (Radnor, PA, USA). The AAV ELISA kits were purchased from Progen (Wayne, PA, USA) while the HEK293 ELISA kits were purchased from Cygnus (Southport, NC, USA). The BioResolve SEC mAb Column (particle diameter: 2.5 µm; pore diameter: 200Å; column diameter: 7.8 mm; column length: 300 mm) size exclusion chromatography column was from Waters Inc. (Milford, MA, USA). The CIMac PrimaS™ 0.1 mL analytical monolith column (diameter: 5.2 mm; length: 4.95 mm; volume: 0.1 mL, channel radius: 1050 nm) for steric exclusion chromatography analysis was obtained from BIA separations (Ajdovscina, Slovenia). The 10-20% Tris-Glycine HCl SDS-PAGE gels were purchased from Bio Rad Life Sciences (Hercules, CA, USA). In house production of AAV6, AAV8, and AAV9 were conducted using plasmids from Aldevron; plasmids pAAV2/9n, pAAV2/8, and pAdDeltaF6 were a gift from James M. Wilson (Addgene plasmid #112865, #112864, and #112867, respectively); pDGM6 was a gift from David Russell (Addgene plasmid #110660);[66] pAAV CAGG eGFP was a gift from Troy Margrie (Addgene plasmid #107707).[67]

***2.3. Synthesis of peptide ligands on Toyopearl resin.*** Sequences CYIHFSGYTNYNPSLKSC (A1), CYIHFSGYTNYNGSLKSC (A2), CYVHFSGYSNYSPSC (A3), CYGHFSGYGNYGPC (A4), CYGHFSPYGNYGPC (A5), CYIHFSGYTNYNPC (A6), CYIHFSPYTNYNPC (A7),

CYHFSYNYPKSC (A8), CYHFSYNYPC (A9), CVIDGSQSTDDDKIC (A10), CDGSQSTDDDKIC (A11), CDSQSTDDDKIC (A12), CSGSTDDDKIC (A13), GYWIGPFTGGGYIHFSGYT (A14), GYWIGPFTGPGYIHFSGYT (A15), GYWIGPFTPGPYIHFSGYT (A16), and LITHPRDYSPKLTPGLYEFG (A17) were synthesized on Toyopearl NH2-750F (TP750F) resin using an Initiator+ Alstra™ automated peptide synthesizer (Biotage, Uppsala, Sweden). Each amino acid coupling step was performed using 3 equivalents (eq.) of Fmoc/tBu-protected amino acid, 3 eq. of HATU and 0.5 M, 6 eq. of DIPEA – all at the concentration of 0.5 M – in dry DMF at 45°C for 20 min. The yield of all amino acid coupling steps was monitored via Kaiser test, while the removal of Fmoc groups was performed using 20% v/v piperidine in DMF at room temperature for 30 min. The final peptide density varied within the range of 0.11 - 0.16 mmol per gram of resin. Following chain elongation, the peptides were deprotected via acidolysis using a cleavage cocktail containing TFA, thioanisole, anisole, and EDT (94/3/2/1) for 2 hrs. After deprotection, the peptide-TP750F resins were washed sequentially with DCM, DMF, methanol, and stored in 20% v/v aqueous methanol.

***2.4. Production and harvest of AAV2 from HEK293 cell cultures.*** Gibco™ Viral Production Cells 2.0 were initially diluted to 3.0 x $10^6$ cells/mL incubated with AAV-MAX Enhancer at 1% v/v in a humidified incubator with 8% $CO_2$ while shaken at 120rpm at 37°C. The transfection cocktail was prepared by combining the pRC2 plasmid, which contains the REP and CAP genes for AAV2, the pHelper plasmid, which contains helper genes necessary for AAV replication, and the pAAV-GFP plasmid, which containing the GFP gene to be packaged into the newly formed AAVs, at the molar DNA ratio of 1:1:1 (pRC2: pHelper: pAAV-GFP) and the total concentration of 1.5 μg per mL of culture. The plasmid cocktail was diluted in Viral-Plex™ Complexation Buffer to 10% of the culture volume. In parallel, volumes of Transfection Booster and Transfection Reagent corresponding to 0.3% and 0.6% of the culture volume were mixed. The DNA/Viral-Plex and the Transfection Booster/Transfection Reagent components were incubated at room temperature for 10 minutes, mixed, and incubated with the Gibco™ Viral Production Cells at room temperature for 20 minutes, after which the cells were returned to the humidified incubator. After 72 hours, AAV-MAX Lysis Buffer was added at a volume corresponding to 10% of the culture volume to lyse cells. The cell lysate was subsequently added with 2 mM $MgCl_2$ and 90 U/mL benzonase endonuclease (GENIUS™ Nuclease) and incubated at 37°C for 2 hours. The lysate was then clarified via centrifugation at 4100g for 40 minutes and the resulting supernatant was collected.

***2.5. Preparation of feed samples.*** Clarified HEK293 cell lysates containing AAV1 and AAV5 were obtained from UNC Vector core (Chapel Hill, NC); clarified HEK293 cell lysates containing AAV2, AAV6, AAV8, and AAV9 were prepared as described in Section 2.4, while the clarified Sf9 cell lysate containing AAV2 was obtained from BTEC (Raleigh, NC). Purified AAV1, AAV2, AAV5, AAV6, AAV8, and AAV9 were prepared at the titer of ~5.0 $10^{11}$ – 5.0 $10^{12}$ vp/mL in 20 mM NaCl in 10 mM Bis-Tris at pH 7.0. The cell culture lysates were diafiltered against 20 mM NaCl in 10 mM Bis-Tris at pH 7.0 to achieve a final AAV2 titer of ~1.9 $10^{12}$ vp/mL, and a HCP titer of ~0.3 mg/mL in the HEK293 harvests and ~1.1 mg/mL in the Sf9 harvest.

***2.6. Binding studies of AAV1, AAV2, AAV5, AAV6, AAV8, and AAV9 in non-competitive conditions using peptide-TP750F resins.*** A volume of 0.5 mL of POROS™ CaptureSelect™ AAVX affinity resin, AVB Sepharose HP resin, (A1) CYIHFSGYTNYNPSLKSC-, (A2) CYIHFSGYTNYNGSLKSC-, (A3) CYVHFSGYSNYSPSC-, (A4) CYGHFSGYGNYGPC-, (A5) CYGHFSPYGNYGPC-, (A6) CYIHFSGYTNYNPC-, (A7) CYIHFSPYTNYNPC-, (A8)

CYHFSYNYPKSC-, (A9) CYHFSYNYPC-, (A10) CVIDGSQSTDDDKIC-, (A11) CDGSQSTDDDKIC-, (A12) CDSQSTDDDKIC-, (A13) CSGSTDDDKIC-, (A14) GYWIGPFTGGGYIHFSGYT-, (A15) GYWIGPFTGPGYIHFSGYT-, (A16) GYWIGPFTPGPYIHFSGYT-, and (A17) LITHPRDYSPKLTPGLYEFG-TP750F resins was initially packed in an Alltech chromatography column and washed with 10 column volumes (CVs) of 20% v/v ethanol, 10 CVs of MilliQ water, and 10 CVs of binding buffer (10 mM Bis-Tris, 20mM NaCl buffer at pH 7.0). A volume of 10 mL of pure AAV solution in binding buffer was loaded on the column at the flow rate of 0.17 mL/min (residence time, RT: 3 min). The resin was washed with 20 CVs of binding buffer at 0.5 mL/min. The bound AAVs were eluted from the peptide-TP750F resins using 1 M $MgCl_2$ in 10 mM Bis-Tris HCl buffer at pH 6.0 at the flow rate of 0.5 mL/min (RT: 1 min); and from POROS™ CaptureSelect™ AAVX affinity resin and AVB Sepharose HP resin respectively using 0.2 M $MgCl_2$ in 200 mM citrate buffer at pH 2.2 and PBS at pH 2.0 at the flow rate of 0.25 mL/min (RT: 2 min). All resins were regenerated with 10 CVs of phosphate buffered saline at pH 2.0 at the flow rate of 0.5 mL/min. All dynamic binding experiments were performed using a ÄKTA Avant system from Cytiva (Marlborough, MA, USA), while continuously monitoring the effluent stream via UV spectrometry at 280 nm. The collected fractions were analyzed using serotype-specific AAV ELISA Kit as described in *Section 2.9* to quantify the values of AAV binding and recovery.

***2.7. Dynamic AAV2 binding capacity of peptide-TP750F resins.*** A volume of 0.5 mL of POROS™ CaptureSelect™ AAVX affinity resin, AVB Sepharose HP resin, (A1) CYIHFSGYTNYNPSLKSC-TP750F resin, (A4) CYGHFSGYGNYGPC-, and (A10) CVIDGSQSTDDDKIC-TP750F resins were initially packed and equilibrated with binding buffer as described in *Section 2.6*. A volume of 45 mL of HEK293 cells lysate containing AAV2 and diafiltered into binding buffer was loaded on the column at the flow rate of 0.17 mL/min (residence time, RT: 3 min). Resin washing and elution of bound AAV2 from the peptide-TP750F resins and the commercial resins was performed as described in *Section 2.6*. All dynamic binding experiments were performed using a ÄKTA Avant system from Cytiva (Marlborough, MA, USA), while continuously monitoring the effluent stream via UV spectrometry at 280 nm. The collected fractions were analyzed by AAV2 ELISA Kit as described in *Section 2.9* to generate the breakthrough curves, and the resulting chromatograms were utilized to calculate the $DBC_{10\%}$.

***2.8. Purification of AAV2 from clarified HEK293 and Sf9 cell lysate using peptide-TP750F resins.*** A volume of 0.5 mL of POROS™ CaptureSelect™ AAVX affinity resin, AVB Sepharose HP resin, (A1) CYIHFSGYTNYNPSLKSC-, (A3) CYVHFSGYSNYSPSC-, (A4) CYGHFSGYGNYGPC-, (A6) CYIHFSGYTNYNPC-, (A10) CVIDGSQSTDDDKIC-, and (A12) CDSQSTDDDKIC-TP750F resins were initially packed and equilibrated with binding buffer as described in *Section 2.6*. A volume of 10 mL of AAV2 at ~$1.9 \cdot 10^{12}$ vp/mL in HEK293 cell culture lysate (HCP titer ~0.3 mg/mL) was loaded at the flow rate of 0.17 mL/min (RT: 3 min). Resin washing and elution of bound AAV2 from the peptide-TP750F resins and the commercial resins was performed as described in *Section 2.6*. All resins were regenerated with 10 CVs of PBS buffer at pH 2.0 at the flow rate of 0.5 mL/min and re-used for 20 additional cycles of AAV2 purification. The collected flow-through and elution fractions were analyzed by ELISA Kit (see *Section 2.9*) to determine the values of AAV2 yield, HEK293 and Sf9 ELISA Kit (see *Section 2.10*) to quantify the values of HCP removal, size exclusion chromatography (see *Section 2.11*) and steric exclusion chromatography (see *Section 2.12*) to measure global product purity, transmission electron

microscopy (see *Section 2.13*) to evaluate the integrity of the eluted AAVs, and fluorescence flow cytometry (see *Section 2.14*) to quantify the transduction efficiency of the eluted AAVs.

***2.9. Capsid quantification via serotype-specific AAV ELISA kits.*** The AAV titer in the feed, flow-through, and elution samples collected as described in *Sections 2.6 - 2.8* was measured using AAV Titration ELISA kit (PROGEN, Wayne, PA) following the manufacturer's protocol.

***2.10. Quantification of HCPs.*** The titer of HEK293 and Sf9 HCPs in the feed, flow-through and elution samples collected as described in *Section 8* was measured using a Generation 3 HEK293 HCP ELISA kit and a Generation 2 Sf9 HCP ELISA kit (Cygnus Technologies, Southport, NC) following the manufacturer's protocols.

***2.11. Analytical size-exclusion chromatography (SEC).*** The feed, flow-through, and elution samples collected as described in *Section 2.8* were analyzed by SEC HPLC using a BioResolve SEC column (Waters, Milford, MA) operated with a 40-min isocratic method using PBS at pH 7.0 (0.05% v/v sodium azide) at the flow rate of 0.50 mL/min. A volume of 10 µL of sample was injected and the effluent continuously monitored via UV (abs: 260 nm and 280 nm) fluorescence spectroscopy (ex/em: 280/350 nm).

***2.12. Analytical steric-exclusion chromatography (SXC).*** The feed, flow-through, and elution samples collected as described in *Section 2.8* were analyzed via analytical SXC using a monolith 0.1 mL CIMac PrimaS™ analytical column (BIA Separations, Slovenia) operated with a 20-min linear gradient from 100:0 A:B to 0:100 A:B (mobile phase A: 10% v/v PEG 6K in PBS at pH 7.0; mobile phase B: 3X PBS at pH 7.0) at the flow rate of 0.33 mL/min. Injection volumes were normalized based on the AAV titer measured via ELISA kits as described in *Section 2.9*. The effluent continuously monitored via fluorescence spectroscopy (ex/em: 280/350 nm).

***2.13. AAV imaging via transmission electron microscopy (TEM).*** The sample grids were glow discharged using the Pelco easiGlow™ unit and taken to a biosafety cabinet, where 3 µL of sample was added on the grid and incubated for 60 seconds at room temperature. Each sample was then blotted using a Whatman paper, and 5 µL of MilliQ water was added on the grid and blotted for 3 times. Finally, 3 µL of 1% v/v Nano-W stain was added on the grid, incubated for 5 seconds, and blotted. The sample grid was dried in a desiccator for 15 minutes and placed in a clean sponge box overnight. The sample grids were imaged using a miniTEM™ system (Vironova, Stockholm, Sweden) using the VIAS software for image collection and analysis.

***2.14. Fluorescence flow cytometry (FFC).*** HT1080 cells were cultured in DMEM media supplemented with 10% v/v FBS at 5% $CO_2$ and 37˚C until reaching 80-90% confluence. Cells were then seeded in 96-well plates at a density of 6,000 cells/well and cultured overnight. The AAV2 in the HEK293 cell lysate and the eluted samples were serially diluted in DMEM (no FBS and antibiotics) added with polybrene at 8 µg/mL. A volume of 0.1 mL of diluted AAV sample was incubated with the HT1080 cells. After 24 hrs, spent medium was replaced with fresh DMEM supplemented with 10% v/v FBS and the cells were cultured for 72 hrs. The fraction of cells expressing GFP ($GFP^+$) was quantified using a CytoFlex flow cytometer (Beckman Coulter, Brea, CA) and the number of transduction units per mL (TU/mL) was calculated using **Equation 1**:

**Equation 1**
$$Activity\left(\frac{TU}{mL}\right) = \frac{N_{HT1080} \times \%GFP^+}{V \times DF}$$

Wherein $N_{HT1080}$ is the number of cells incubated with the diluted AAV sample, $V$ is the volume of the diluted AAV sample, and $DF$ is the dilution factor.

## 3. Results and Discussion

### 3.1. Rational design of AAVR-mimetic and A20-mimetic peptides

A number of biological ligands targeting AAV are known to date, including transmembrane receptor proteins and engineered proteins. Tissue targeting and cell access by AAVs is mediated by attachment factors, namely glycan moieties (*e.g.*, sucrose octasulfate, sialic acid, and galactose), also known as 'primary receptors', which feature promiscuous low-affinity capsid binding and whose role is to accumulate AAV at the cell surface; and cell surface receptors that specifically interact with AAV and whose binding is required to initiate viral cell entry. To date, known receptors and their target serotypes include oligosaccharide heparin (AAV2) and fondaparinux (AAV-DJ) as well as the AAV receptor (AAVR, also known as KIAA0319L), a 150 kDa glycoprotein required for cell transduction by several serotypes, including AAV1, AAV2, AAV3B, AAV5, AAV6, AAV8, and AAV9. The ectodomain of AAVR comprises multiple domains, known as Ig-like polycystic kidney disease repeat domains (PKD):[32,33] for example, AAV2 is bound by PDK1-3, AAV5 predominantly interacts with PKD1, while AAV1 and AAV8 require a combination of PKD1 and PKD2. Additionally, AAV2 targets integrins, fibroblast growth factor receptor (FGFR1), αVβ5, and α5β1;[34-36] AAV2, AAV3, AAV8, and AAV9 capsid proteins have been found to bind the laminin receptor displayed on the surface of yeast cells;[37]AAV2 and AAV3 bind FGFR1,[35,38] the hepatocyte growth factor receptor (HGFR),[39] while AAV5 and AAV6 respectively target the platelet-derived growth factor receptor (PDGFR) and the epidermal growth factor receptor (EGFR).[40] Besides natural receptors, a number of anti-AAV monoclonal neutralizing antibodies have been developed, including mNAbs ADK1a, 4E4, and ADK6 targeting AAV1, mNAbs A20 and C37-B targeting AAV2, mNAbs ADK5b and HL2476 and mAbs ADK5a and 3C5 targeting AAV5, and mNAbs ADK5a and ADK6 targeting AAV6, and mAb ADK8 targeting AAV8. Finally, single chain camelid antibody fragments and small protein scaffolds have been developed as affinity ligands for purifying AAVs from recombinant cell lysates, including serotype-agnostic AAVX, AAV8- and AAV9-targeted CSAL8 and CSAL9 developed by ThermoFisher; serotype-agnostic AVB by Cytiva; and AVIPure® AAV2, AAV8, and AAV9 for the corresponding serotypes.

Despite the abundance of AAV-binding ligands, only the crystal structures of AAVR in complex with AAV1 (PDB ID: 6JCQ and 7TI5), AAV2 (6IHB and 6NZ0), AAV5 (6JCS), and AAV9 (7WJX) as well as the complex of AAV2 with monoclonal antibody A20 (3J1S) are reported. The analysis of pairwise interactions between the active residues on AAVR and A20 and the targeted residues on the virion protein (VP1), reported in **Figure S1** and **Table S1**, identified critical AAV-binding residues and motifs. These were utilized to design an *in silico* ensemble of candidate ligands, whose sequence, structure, and key physicochemical parameters are reported in **Table S2**. As can be gathered from the sequence homology and the values of root-mean-square deviation (RMSD) of the atomic positions of the peptides *vs.* their cognate proteins, the proposed library spans a wide space of chemical and structural diversity as well as different levels of similarity with A20 and AAVR.

The peptides were docked *in silico* against the homology spherical cap structures of AAV1, AAV2, AAV5, AAV6, AAV8, and AAV9. These were created by collating the published structures of VP1 into the triangular asymmetric units that form the icosahedral AAV capsid.[9] Prior to docking, the triangular clusters were equilibrated to two values of pH – 7.4, which is utilized during adsorption, and 6.0, which is adopted for the product release. An initial round of "blind" docking was performed to evaluate the ability of the designed sequences to target the

known binding sites of A20 and AAVR. In order to mimic the orientational constraint imposed upon the peptides by their conjugation onto the surface of the chromatographic resin, the -GSG tripeptide appended on the C-terminal end of the peptides was constrained not to bind AAV[13,17,19,41-47]. Selected AAV:peptide complexes (those comprising more than 20 peptide clusters) were refined via 250-ns MD simulations in explicit solvent at both pH 7.4 and 6.0 to obtain reliable values of binding free energy ($\Delta G_b$). Representative complexes formed by the selected peptides on the target serotypes are shown in **Figure 1**, while the values of binding energy and the corresponding dissociation constant ($K_{D,in\ silico}$) are listed in **Tables 1** and **2**; finally, detailed results of A1, A4, and A10 docking on the target AAV1, AAV2, AAV5, AAV6, AAV8, and AAV9 are reported in **Figures S2**.

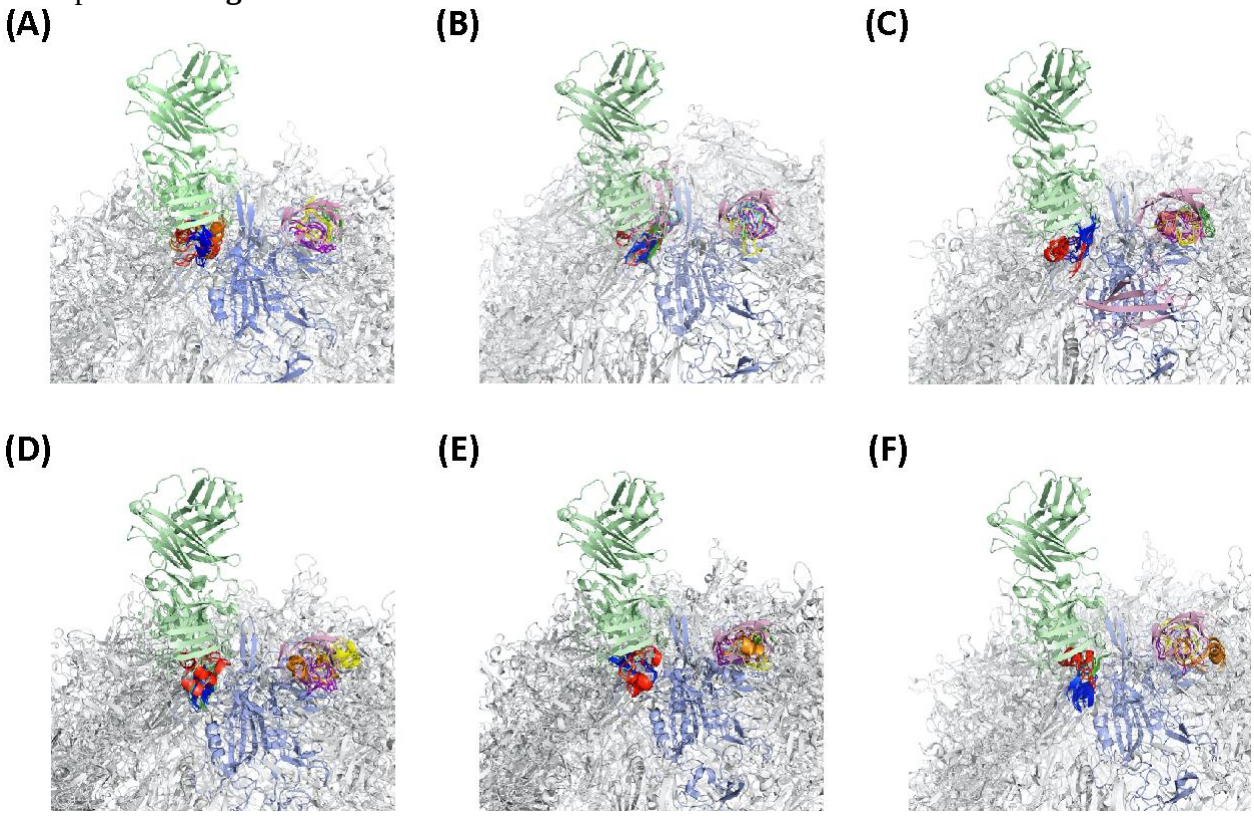


***Figure 1.*** *Representative complexes formed by A20-mimetic peptides CYIHFSGYTNYNPSLKSC (A1, red), CYGHFSGYGNYGPC (A4, green), CYIHFSGYTNYNPC (A6, blue), CVIDGSQSTDDDKIC (A10, yellow), CDGSQSTDDDKIC (A11, magenta), and LITHPRDYSPKLTPGLYEFG (A17, orange) with the capsids of* ***(A)*** *AAV1 (PDB IDs: 6JCQ, 6JCR, 7RK9, and 8FQ4),* ***(B)*** *AAV2 (5IPI, 6IH9, 6IHB, and 6U0V);* ***(C)*** *AAV5 (6JCS, 6JCT, 7KP3, and 7KPN);* ***(D)*** *AAV6 (3SHM, 3OAH, 4V86, and 5EGC);* ***(E)*** *AAV8 (2QA0, 3RAA, 6PWA, 6U2V, and 6V10); and* ***(F)*** *AAV9 (3UX1, 7MT0, 7WJW, and 7WJX) obtained via molecular docking and dynamics simulations at pH 7.4 and ionic strength of 150 mM. The AAVR and the A20 antibody are presented as light pink and light green cartoons, respectively; the VP1 is presented as light blue cartoon, while the remainder of the capsid is presented in light gray cartoon.*

***Table 1.*** *Values of dissociation constant ($K_{D,in\ silico}$) of the complexes formed by A20-mimetic peptides with the capsids of AAV1, AAV2, AAV5, AAV6, AAV8, and AAV9 obtained via molecular docking and dynamics simulations at pH 7.4 and ionic strength of 150 mM and at pH 6.0 and ionic strength of 2 M. †: not available.*

| **A20-mimetic Sequence** | **AAV1:peptide $K_{D,in\ silico}$ (M)** | | **AAV2:peptide $K_{D,in\ silico}$ (M)** | | **AAV5:peptide $K_{D,in\ silico}$ (M)** | | **AAV6:peptide $K_{D,in\ silico}$ (M)** | | **AAV8:peptide $K_{D,in\ silico}$ (M)** | | **AAV9:peptide $K_{D,in\ silico}$ (M)** | |
|---|---|---|---|---|---|---|---|---|---|---|---|---|
| | **pH 6.0** | **pH 7.4** | **pH 6.0** | **pH 7.4** | **pH 6.0** | **pH 7.4** | **pH 6.0** | **pH 7.4** | **pH 6.0** | **pH 7.4** | **pH 6.0** | **pH 7.4** |
| CYIHFSGYTNYNPSLKSC (A1) | $8.81\cdot10^{-4}$ | $2.16\cdot10^{-6}$ | $7.91\cdot10^{-4}$ | $6.12\cdot10^{-7}$ | $3.83\cdot10^{-3}$ | $1.84\cdot10^{-6}$ | $5.28\cdot10^{-4}$ | $2.54\cdot10^{-7}$ | $4.95\cdot10^{-4}$ | $6.26\cdot10^{-6}$ | $1.27\cdot10^{-4}$ | $6.27\cdot10^{-6}$ |
| CYIHFSGYTNYNGSLKSC (A2) | $4.88\cdot10^{-4}$ | $1.10\cdot10^{-6}$ | $4.69\cdot10^{-4}$ | $1.07\cdot10^{-6}$ | $4.59\cdot10^{-4}$ | $1.08\cdot10^{-6}$ | $1.04\cdot10^{-4}$ | $1.10\cdot10^{-6}$ | $4.59\cdot10^{-4}$ | $1.03\cdot10^{-6}$ | $4.56\cdot10^{-4}$ | $1.09\cdot10^{-6}$ |
| CYVHFSGYSNYSPSC (A3) | $1.75\cdot10^{-3}$ | $9.65\cdot10^{-5}$ | $4.27\cdot10^{-4}$ | $7.47\cdot10^{-7}$ | $5.67\cdot10^{-4}$ | $8.58\cdot10^{-6}$ | $4.43\cdot10^{-4}$ | $2.84\cdot10^{-6}$ | $7.47\cdot10^{-5}$ | $4.28\cdot10^{-6}$ | $1.09\cdot10^{-4}$ | $5.41\cdot10^{-5}$ |
| CYGHFSGYGNYGPC (A4) | $5.70\cdot10^{-4}$ | $2.64\cdot10^{-5}$ | $6.53\cdot10^{-4}$ | $6.17\cdot10^{-6}$ | $1.26\cdot10^{-4}$ | $3.72\cdot10^{-5}$ | $5.26\cdot10^{-4}$ | $1.38\cdot10^{-6}$ | $4.50\cdot10^{-4}$ | $3.44\cdot10^{-6}$ | $2.64\cdot10^{-4}$ | $4.39\cdot10^{-6}$ |
| CYGHFSPYGNYGPC (A5) | $7.21\cdot10^{-4}$ | $4.18\cdot10^{-5}$ | $7.27\cdot10^{-4}$ | $4.21\cdot10^{-5}$ | $7.77\cdot10^{-4}$ | $4.20\cdot10^{-5}$ | $4.32\cdot10^{-4}$ | $4.36\cdot10^{-5}$ | $7.64\cdot10^{-4}$ | $4.18\cdot10^{-5}$ | $7.34\cdot10^{-4}$ | $4.15\cdot10^{-5}$ |
| CYIHFSGYTNYNPC (A6) | $8.77\cdot10^{-4}$ | $8.01\cdot10^{-5}$ | $8.27\cdot10^{-4}$ | $1.34\cdot10^{-6}$ | $8.31\cdot10^{-4}$ | $9.12\cdot10^{-5}$ | $4.74\cdot10^{-4}$ | $2.20\cdot10^{-6}$ | $4.06\cdot10^{-4}$ | $3.47\cdot10^{-5}$ | $1.21\cdot10^{-4}$ | $4.56\cdot10^{-5}$ |
| CYIHFSPYTNYNPC (A7) | $1.09\cdot10^{-4}$ | $6.31\cdot10^{-5}$ | $5.21\cdot10^{-5}$ | $2.45\cdot10^{-5}$ | $9.24\cdot10^{-5}$ | $5.87\cdot10^{-5}$ | $4.01\cdot10^{-5}$ | $2.54\cdot10^{-5}$ | $8.03\cdot10^{-5}$ | $4.60\cdot10^{-5}$ | $1.04\cdot10^{-4}$ | $4.50\cdot10^{-5}$ |
| CYHFSYNYPKSC (A8) | $5.89\cdot10^{-4}$ | $1.57\cdot10^{-5}$ | $5.99\cdot10^{-4}$ | $1.65\cdot10^{-5}$ | $6.18\cdot10^{-4}$ | $1.72\cdot10^{-5}$ | $1.66\cdot10^{-4}$ | $1.59\cdot10^{-5}$ | $5.79\cdot10^{-4}$ | $1.67\cdot10^{-5}$ | $6.15\cdot10^{-4}$ | $1.59\cdot10^{-5}$ |
| CYHFSYNYPC (A9) | $6.79\cdot10^{-4}$ | $2.84\cdot10^{-5}$ | $6.61\cdot10^{-4}$ | $2.87\cdot10^{-5}$ | $6.85\cdot10^{-4}$ | $2.94\cdot10^{-5}$ | $2.82\cdot10^{-4}$ | $2.92\cdot10^{-5}$ | $7.03\cdot10^{-4}$ | $2.87\cdot10^{-5}$ | $6.84\cdot10^{-4}$ | $2.98\cdot10^{-5}$ |
| A20 | † | | $3.68\cdot10^{-7}$ | $9.30\cdot10^{-8}$ | † | | | | | | | |

***Table 2.*** *Values of dissociation constant ($K_{D,in\ silico}$) of the complexes formed by AAVR-mimetic peptides with the capsids of AAV1, AAV2, AAV5, AAV6, AAV8, and AAV9 obtained via molecular docking and dynamics simulations at pH 7.4 and ionic strength of 150 mM and at pH 6.0 and ionic strength of 2 M. †: not available.*

| **AAVR-mimetic Sequence** | **AAV1:peptide $K_{D,in\ silico}$ (M)** | | **AAV2:peptide $K_{D,in\ silico}$ (M)** | | **AAV5:peptide $K_{D,in\ silico}$ (M)** | | **AAV6:peptide $K_{D,in\ silico}$ (M)** | | **AAV8:peptide $K_{D,in\ silico}$ (M)** | | **AAV9:peptide $K_{D,in\ silico}$ (M)** | |
|---|---|---|---|---|---|---|---|---|---|---|---|---|
| | **pH 6.0** | **pH 7.4** | **pH 6.0** | **pH 7.4** | **pH 6.0** | **pH 7.4** | **pH 6.0** | **pH 7.4** | **pH 6.0** | **pH 7.4** | **pH 6.0** | **pH 7.4** |
| CVIDGSQSTDDDKIC (A10) | $3.84\cdot10^{-4}$ | $1.18\cdot10^{-5}$ | $4.66\cdot10^{-4}$ | $4.15\cdot10^{-6}$ | $6.11\cdot10^{-4}$ | $9.83\cdot10^{-6}$ | $5.41\cdot10^{-4}$ | $1.29\cdot10^{-5}$ | $2.21\cdot10^{-4}$ | $8.06\cdot10^{-6}$ | $6.78\cdot10^{-4}$ | $3.08\cdot10^{-6}$ |
| CDGSQSTDDDKIC (A11) | $3.75\cdot10^{-4}$ | $1.10\cdot10^{-5}$ | $5.31\cdot10^{-4}$ | $2.92\cdot10^{-6}$ | $6.98\cdot10^{-4}$ | $9.90\cdot10^{-5}$ | $4.10\cdot10^{-4}$ | $1.93\cdot10^{-6}$ | $3.28\cdot10^{-4}$ | $7.29\cdot10^{-5}$ | $3.16\cdot10^{-4}$ | $7.97\cdot10^{-6}$ |
| CDSQSTDDDKIC (A12) | $1.58\cdot10^{-4}$ | $1.29\cdot10^{-4}$ | $5.43\cdot10^{-4}$ | $1.40\cdot10^{-6}$ | $5.71\cdot10^{-4}$ | $9.62\cdot10^{-5}$ | $3.45\cdot10^{-4}$ | $1.56\cdot10^{-6}$ | $2.37\cdot10^{-4}$ | $7.28\cdot10^{-5}$ | $3.52\cdot10^{-4}$ | $8.01\cdot10^{-6}$ |
| CSGSTDDDKIC (A13) | $9.45\cdot10^{-4}$ | $1.03\cdot10^{-4}$ | $5.80\cdot10^{-4}$ | $1.59\cdot10^{-6}$ | $3.23\cdot10^{-4}$ | $1.24\cdot10^{-5}$ | $3.59\cdot10^{-4}$ | $1.63\cdot10^{-6}$ | $2.06\cdot10^{-4}$ | $7.16\cdot10^{-5}$ | $4.40\cdot10^{-4}$ | $8.56\cdot10^{-6}$ |
| GYWIGPFTGGGYIHFSGYT (A14) | $3.52\cdot10^{-3}$ | $7.58\cdot10^{-5}$ | $3.81\cdot10^{-4}$ | $7.57\cdot10^{-5}$ | $2.82\cdot10^{-3}$ | $7.26\cdot10^{-5}$ | $2.80\cdot10^{-3}$ | $7.82\cdot10^{-5}$ | $2.80\cdot10^{-3}$ | $7.82\cdot10^{-5}$ | $2.66\cdot10^{-3}$ | $7.78\cdot10^{-5}$ |
| GYWIGPFTGPGYIHFSGYT (A15) | $6.80\cdot10^{-3}$ | $4.81\cdot10^{-5}$ | $6.37\cdot10^{-3}$ | $4.95\cdot10^{-5}$ | $3.69\cdot10^{-3}$ | $4.98\cdot10^{-5}$ | $3.82\cdot10^{-3}$ | $4.73\cdot10^{-5}$ | $3.84\cdot10^{-3}$ | $4.98\cdot10^{-5}$ | $3.76\cdot10^{-3}$ | $4.74\cdot10^{-5}$ |
| GYWIGPFTPGPYIHFSGYT (A16) | $3.08\cdot10^{-3}$ | $6.30\cdot10^{-5}$ | $3.23\cdot10^{-3}$ | $6.71\cdot10^{-5}$ | $2.14\cdot10^{-3}$ | $6.61\cdot10^{-5}$ | $2.09\cdot10^{-3}$ | $6.73\cdot10^{-5}$ | $2.22\cdot10^{-3}$ | $6.63\cdot10^{-5}$ | $2.15\cdot10^{-3}$ | $6.38\cdot10^{-5}$ |
| LITHPRDYSPKLTPGLYEFG (A17) | $4.95\cdot10^{-3}$ | $2.71\cdot10^{-5}$ | $4.70\cdot10^{-3}$ | $2.75\cdot10^{-5}$ | $1.01\cdot10^{-3}$ | $2.74\cdot10^{-5}$ | $9.98\cdot10^{-3}$ | $2.77\cdot10^{-5}$ | $1.02\cdot10^{-3}$ | $2.70\cdot10^{-5}$ | $1.02\cdot10^{-3}$ | $2.72\cdot10^{-5}$ |
| AAVR | $1.40\cdot10^{-5}$ | $1.80\cdot10^{-6}$ | $1.17\cdot10^{-5}$ | $1.60\cdot10^{-6}$ | $9.01\cdot10^{-6}$ | $1.71\cdot10^{-6}$ | † | | | | $3.57\cdot10^{-6}$ | $1.70\cdot10^{-6}$ |

Our *in silico* results show that a significant fraction of the designed peptides – 17 sequences out of the 28 originally designed and listed in *Section 2.1* – were found to bind all target serotypes, forming binding poses that overlap with those of the AAVR:AAV and A20:AAV2 complexes (**Figure 1**). Most notably, nine A20-mimetic peptides formed true affinity interactions ($|\Delta G_b| > 6.5$ kcal/mol at pH 7.4) with all serotypes, despite the cognate A20 being designed as an anti-AAV2 antibody: this can be attributed to the cyclic format of these candidate ligands, whose rigidity decreases the entropic penalty to the binding energy that is characteristic of their linear, and hence more flexible, counterparts; as anticipated, however, shorter sequences (A5 – A9) exhibited lower binding energies (binding energy $|\Delta G_b| < 7.5$ kcal/mol) than longer variants (A1 – A4), whose higher number of amino acids provides a stronger enthalpic contribution to the binding energy. Particularly notable was the case of CYIHFSGYTNYNPSLKSC (A1), whose dominant binding site on AAV1, AAV2, AAV5, AAV6, and AAV8 ($|\Delta G_b|$ ~7.7 - 9 kcal/mol at pH 7.4) shares > 90% of paired interactions with A20. We also noted that the shortest A20-mimetics (A6 – A9) showed the ability to form multiple low-affinity binding poses on the various serotypes that do not overlap with the binding sites of either A20 or AAVR. This can be imputed to their smaller hydrodynamic radius (**Table S2**), which enables these peptides to fit druggable sites displayed on the capsid surface that are precluded to larger binders. As observed in a prior study,[9] the solvent-accessible convex surface of AAV capsids present multiple sites that are highly conserved across serotypes and "ligandable" (*i.e.*, and whose physicochemical features – namely, pocket surface and volume as well as balance of electrostatic, hydrophobic and hydrogen bond-forming residues – are suitable to accommodate peptide ligands); since the target regions of AAVR and A20 are included in the list of ligandable sites, it did not surprise that A20-mimetic peptides interact with multiple sites on all serotypes. At the same time, this also suggests the possibility for smaller A20-mimetic peptides to interact with host cell proteins (HCPs) and other impurities in the feedstock, thus reducing their binding selectivity and thwarts their candidacy for experimental evaluation.

Analogous results were observed with the AAVR-mimetic sequences. Among them, CVIDGSQSTDDDKIC (A10) and its derivatives A11 – A13 featured affinity-like interactions ($|\Delta G_b|$ ~6.5 – 7.7 kcal/mol at pH 7.4) with all target serotypes, especially AAV2, AAV5, AAV6, AAV8, and AAV9, with which they formed binding poses that share > 90% of paired interactions with AAVR. Once again, shorter variants, chiefly A12 and A13 were found to form multiple yet low-affinity interactions with multiple sites, besides the epitopes of A20 and AAVR, suggesting their ability to act as promiscuous binders, and thus as ligands with poor selectivity.

While the predicted affinity of these sequences was found to be consistently lower than that of A20-mimetics, we note that the binding strength of the AAV:AAVR complexes whence these peptides were derived is originally lower than that of the AAV2:A20 complex. Furthermore, a milder binding strength does not necessarily translate into weaker binding: as we noted in prior work,[9] the peptide density on the surface of the resin is sufficient to form multiple interactions with a single capsid, wherein multiple affinity interactions with modest binding energy are synergized into a strong avidity-like binding that efficient AAV capture (*note:* the values of peptide density on the resin (~0.12 – 0.15 mmol per gram), the resin's specific surface (~30 $m^2/g$), and the projection area of the triangular unit formed by 3 VPs on the icosahedral capsid (~81 $nm^2$), in fact, suggest that up to 30 peptides are displayed on pore surface that is impacted by a single capsid, enabling the formation of 3 - 5 VP:peptide interactions per bound capsid). Finally, moderate binding strength is welcome in the context of affinity purification of AAVs, since weak VP:peptide interactions reduce the risk of irreversible adsorption and promote an easier elution of the capsids, thus safeguarding their tissue tropism and transduction activity.

These observations motivate the selection of sequences whose binding energy decreases to ~4 – 5 kcal/mol as the pH decreases from pH 7.4 to 6.0 and the ionic strength of the aqueous environment increases to 2 M (representing the transition from the adsorption step conducted in PBS at pH 7.4 to the elution step in 1 M $MgCl_2$ at pH 6.0). This translates in a 120-to-330-fold shift in the dissociation constant for A20-mimetics ($K_D$, **Table 1**) and a 30-to-190-fold shift in the $K_D$ of AAVR-mimetics (**Table 2**). A20-mimetics A1 – A4 and AAVR-mimetics A10 – A12 are the sequences with the strongest variation in binding energy ($\Delta\Delta G_b$ > 3 kcal/mol, translating in a $\Delta K_D$ > 150-fold increase), and thus the highest likelihood of releasing the bound capsids under the desired conditions. The mechanism of VP:peptide dissociation portrayed by the MD simulations is a combined results of the variation in pH and ionic strength. Contrary to what generally observed with peptide ligands, the Coulombic interactions formed by A20 and its mimetics A1 – A4 provided a rather minor contribution (11-15%) to the binding energy at pH 7.4: the only interactions found were formed by cationic Lys in A1 and A2 with Asp514 and Asp 711 on AAV1, Asp269 and Asp 711 on AAV2, Asp704 on AAV5, Asp268 on AAV6, Asp270 on AAV8, and Asp231 on AAV9; conversely, A3 and A4 do not contain ionizable residues (except His, which is neutral at pH 7.4); finally, the triplet (DDD) of A10 – A12 only targeted Lys508 on AAV1 and AAV2, Lys501 on AAV5, Lys507 on AAV6, and Lys509 on AAV8. Conversely, a strong network of hydrogen bonds and polar interactions formed by the side chains of Ser and Thr, Asn and Gln, His, Asp, and Tyr residues as well as the backbone amide bonds contribute ~65-74% of the binding energy. Finally, moderate hydrophobic interactions and π-π stacking occur, which account for ~16-24% of the binding energy. Finally, we noted that the acidification of the environment to pH 6 causes a minor rearrangement in the capsid structure, together with softening most of the electrostatic interactions, whereas the addition of $MgCl_2$ – a known chaotrope – destabilizes the electrostatic, hydrophobic, and hydrogen bonding interactions that maintain the native VP conformation and its interaction with the surface-bound peptide ligands, ultimately triggering the release of the capsid. These phenomena are observed mostly with the VP:A2, VP:A3, and VP:A10 complexes, whose binding strength at pH 7.4 is moderate (*i.e.*, 7.6 > $|\Delta G_b|$ > 6.5 kcal/mol) and undergoes the sharpest change upon switching from binding to the elution conditions. For reference, the VP:A20 complex features an *in silico* $\Delta G_b$ ~8.4 kcal/mol and drops by only 1.2 kcal/mol upon elution; the binding strength of AAV:AAVR complexes, while more modest, exhibits no-to-little dependence upon either pH or ionic strength within the explored ranges, and are therefore unlikely to afford sufficient product yield upon mild elution conditions.

In summary, these results support the adoption of small cyclic peptides as ligands for AAV purification via affinity chromatography: *(i)* with multiple μM-level affinity interactions cooperating into sub-nM avidity capture, peptide-functionalized adsorbents can match their protein-based counterparts in terms of binding capacity and selectivity; *(ii)* small pH variations or additions of chaotropes that disrupt the single VP:peptide interaction are sufficient to trigger capsid release; conversely, mild elution conditions only marginally affect VP:protein interactions, which require much stronger stimuli, resulting in a loss of yield and transduction activity of the recovered capsids as well as a shorter resin lifetime (*note:* irreversible multi-site VP:proteins interactions may in fact form a fouling film of bound capsids, which builds up across multiple uses and results in the short lifetime characteristic of commercial adsorbents).

### 3.2. Evaluation of AAV binding by the designed peptide ligands in non-competitive mode

The results of molecular docking and dynamics of designed peptides on multiple serotypes yielded a shortlist of sequences – namely, A20-mimetic peptides CYIHFSGYTNYNPSLKSC (A1),

CYVHFSGYSNYSPSC (A3), CYGHFSGYGNYGPC (A4), and CYIHFSGYTNYNPC (A6), and AAVR-mimetic peptides CVIDGSQSTDDDKIC (A10) and CDSQSTDDDKIC (A12) – to be evaluated in dynamic mode against target serotypes AAV1, AAV2, AAV5, AAV6, AAV8 and AAV9. These targets belong to different clones (AAV5) or clades[48,49] – namely A (AAV1 and AAV6), B (AAV2), E (AAV8), and F (AAV9) – and were selected for their outstanding therapeutic value: serotypes 1 and 2 target skeletal, muscle and cardiac cells, and are currently utilized in clinical trials against heart failure, Pompe disease, Hemophilia B, and AAT deficiency;[50] serotypes 1, 2, 5, 8, 9 target the cells in the central nervous system, especially neurons, and are currently being tested in clinical trials against Alzheimer, Canavan, and Parkinson diseases;[51] finally, serotypes 6 targets epithelial, skeletal cells, and hepatocytes, while serotype 8 targets cardiac cells, skeletal cells, hepatocytes. Notably, affinity resins marketed as serotype-agnostic show excellent binding of AAV1, AAV2, AAV5, and AAV6, but may struggle to capture AAV8 and AAV9, and dedicated adsorbents for their purification have been developed. Accordingly, the model AAVs adopted in this study, while only representing half of the wild serotypes, provide a broad coverage of the AAV atlas and thus adequate evaluation of the AAV-targeting activity of the designed sequences.

The peptides were conjugated on Toyopearl NH2-750F resin, whose large pore diameter (> 100 nm) and small particle size ensures efficient AAV transport into and binding onto the adsorbent pores. To evaluate the peptide-based resins under conditions that are representative of biopharmaceutical processes, the feedstocks were formulated as pure AAVs at ~$5.0 \cdot 10^{11}$ - $5.0 \cdot 10^{12}$ vp/mL in 10 mM Bis-Tris buffer at pH 7.0 and loaded at the ratio of ~$10^{13}$ vp per mL of resin (the expected to be the average binding capacity of the resins). To ensure a stringent evaluation of the performance of peptide-based adsorbents, the bound AAVs were eluted from the peptide-Toyopearl resins under the same conditions adopted for peptide design – namely, 1 M $MgCl_2$ in 10 mM Bis-Tris buffer at pH 6.0 – whereas a strong acidic buffer (*i.e.*, 200 mM $MgCl_2$ in 200 mM citrate buffer at pH 2.2 and PBS at pH 2.0, respectively, as recommended by the manufacturers) was used for elution from the POROS™ CaptureSelect™ AAVX and AVB Sepharose HP resins used as reference adsorbents. The values of product loss (*i.e.*, in the flow-through fractions) and yield are summarized in **Figure 2**.

As shown in **Figure 2**, the selected peptide resins, and particularly A1-Toyopearl, displayed broad AAV-binding activity. Particularly efficient is the binding of AAV2, which, followed by AAV6, was the serotype most efficiently captured. These results align with the rationale of ligand design, which leverages the known epitopes on AAVR and A20 – both AAV2-binding proteins. Among the tested sequences, negligible values of product loss during loading and remarkable values of yield at pH 6.0 were provided by peptides A1 (0.14% and 71.4%, respectively), A4 (0.2% and 61.6%), and A6 (1.36%, 79.7%), which outperformed AAVX POROS™ (1.27% and 63.4%) and AVB Sepharose (0.2%, 45.8%) resins. Notably, the *in silico* results suggest that the list of binding sites of these peptides include, besides those targeted by AAVR and A20, two epitopes located on VP surface and distance from the VP:VP interface. The availability of neighboring binding sites promotes capsid capture, translating in higher values of capacity and lower loss during loading. At the same time, the significant drop in binding strength upon mild acidification is also coherent with the excellent values of product recovery. Supporting the efficient capture of AAV2 by almost all peptides is also the propensity of this serotype to aggregate into soluble multimeric constructs, which further promotes multi-site interactions with the peptide-functionalized surface.

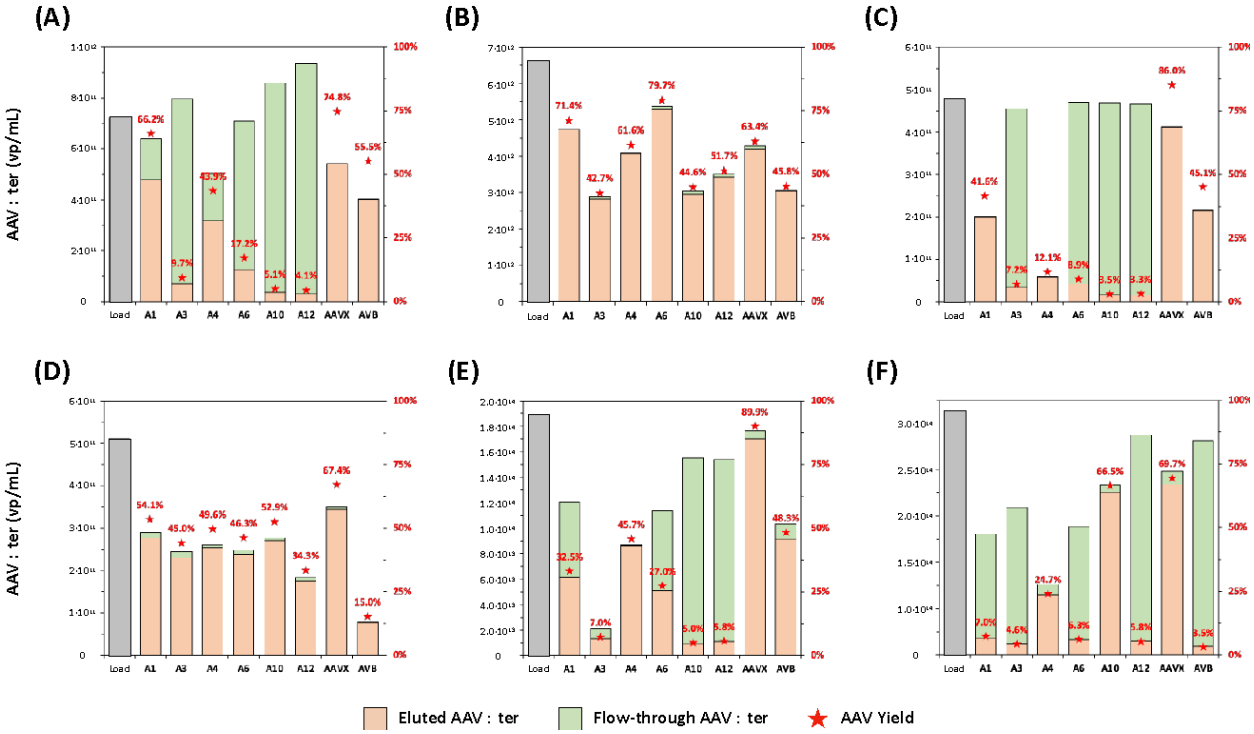


***Figure 2.*** *Values of loss (orange, calculated as the ratio of the AAV titer in the flow-through and wash fractions vs. load) and yield (green, calculated as the ratio of the AAV titer in the elution fraction vs. load) of* ***(A)*** *AAV1,* ***(B)*** *AAV2,* ***(C)*** *AAV5,* ***(D)*** *AAV6,* ***(E)*** *AAV8 and* ***(F)*** *AAV9 obtained via bind-and-elute studies in non-competitive mode using peptide-based resins (A1) CYIHFSGYTNYNPSLKSC-, (A3) CYVHFSGYSNYSPSC-, (A4) CYGHFSGYGNYGPC-, (A6) CYIHFSGYTNYNPC-, (A10) CVIDGSQSTDDDKIC- and (A12) CDSQSTDDDKIC-Toyopearl resins, and control adsorbents POROS™ CaptureSelect™ AAVX (AAVX) and AVB Sepharose HP (AVB) resins. The AAV titer in the flow-through, wash, and elution fractions was measured using serotype-specific ELISA kits.*

Efficient binding and recovery were also observed with AAV1, AAV6, and AAV8. In particular, peptides A1 and A4 afforded excellent binding and gentle release of AAV1 and AAV6: the values of product yield were respectively 66.2 and 54.1% with A1-Toyopearl resin, which performed comparably to AAVX POROS™ resin (74.8 and 67.4%) and outperformed AVB Sepharose (55.5 and 15.0%); and 43.9% and 49.6% with A4-Toyopearl resin. Both serotypes belong to Clade A, which is closely related to Clade B, to which AAV2 belongs: AAV1 and AAV6 feature, in fact, a 91-92% structural homology with AAV2 (*note:* sequence homology, however, is 81-83%). With structural complementarity playing a key role in AAV docking on the peptide-functionalized surface, it stands to reason that structural homology is an underlying factor of AAV1/2/6 binding shared by these three sequences.

Peptides A1 and A4 also showed a similar performance with AAV8, affording product yield of 32.5% and 45.7% respectively, followed by A6 with 27%. Notably, AA8 (Clade E) exhibits a 94% structural homology, but only 82% sequence homology, with AAV2. When tested against AAV9, however, only A4 maintained acceptable product recognition with only 4.2% loss and 24.7% yield; conversely, A1 only afforded 7% yield and significant product loss. Notably, A10 returned a remarkable yield of 66.5%, comparable with that of AAVX POROS™ resin (69.7%) and significantly higher than that of AVB Sepharose resin (3.5%).

As anticipated, the capture of AAV5 proved the most challenging: the most unique among all AAVs, AAV5 exhibits a poor structural (58-71%) and sequence (58-79%) homology with the

other serotypes evaluated in this study. It is therefore remarkable that peptide A1 captured (0.2% loss) and released it efficiently (41.6% yield).

Three general conclusions can be drawn from the experimental evaluation of the *in silico*-selected peptides. First, peptide CYGHFSGYGNYGPC (A4) performed well with all serotypes, exhibiting negligible product loss, thus suggesting that the variations in yield should be attributed to differences in binding strength to the various serotypes. A comparative evaluation of the values of $K_D$ measured *in silico* (**Table 1**) and the experimental values of AAV yield, in fact, show that high yields (45 - 80%) were obtained when a >100-fold increase in $K_D$ was registered (AAV2, AV6, and AAV8), whereas moderate yields (25 - 44%) were obtained when only a 10-to-50 fold increase was registered (AAV1 and AAV9); finally, the lowest yield, obtained with AAV5, coincided with a mere 3-fold increase in $K_D$. A similar comparison can be made for the second best sequence CYIHFSGYTNYNPSLKSC (A1), whose high yield of AAV1, AAV2, and AAV6 coincided respectively with a 400-, 130-, and 2080-fold increase in $K_D$, while the product loss and lower yield registered with AAV8 and AAV9 coincided with both a lower binding strength and a lower shift in $K_D$. Shifts in affinity of such magnitude under mild acidification (pH 6) are hardly attainable with protein ligands, which require much harsher environments to release the bound capsids, and justify the choice of peptide ligands for the purification of labile products such as viral vectors. Secondly, peptides A3, A6, and A12 behaved differently with different serotypes, affording excellent capture and yield of AAV2 and AAV6, but high product loss and consequently low yield of AAV1, AAV5, AAV8, and AAV9. Notably, the low capture of these serotypes is matched by the *in silico* results, which predicted a low binding strength of these peptides at pH 7.4 ($K_D > 3.5\ 10^{-5}$ M); conversely, a higher binding strength ($K_D$ ~$7.5\ 10^{-7}$ M – $2.8\ 10^{-6}$ M) was predicted for AAV2 and AAV6, suggesting that, while moderate affinity is still desirable, binding strength must be above a minimum threshold to ensure sufficient product capture. On the other hand, the serotypes that were poorly captured by A3, A6, and A12 were effectively recovered using A1 and A4, thus prompting the choice of discontinue these peptides. Thirdly, sequence CVIDGSQSTDDDKIC (A10) performed uniquely well with AAV9, on par with AAVX POROS™ resin, while outperforming all other peptide-based resins and AVB Sepharose; once again, the performance of the peptide is inscribed in the values of binding strength at pH 7.4 ($K_D$ ~$3.08 \cdot 10^{-6}$ M) and strong affinity loss (220-fold increase in $K_D$) upon acidification predicted *in silico*. Under the light of these results, peptides A1, A4, and A10 were carried forward for additional experimental evaluation.

### 3.3. Purification of AAV2 from HEK293 and Sf9 cell lysates

We moved to evaluate the three selected peptide-based adsorbents A1-, A4-, and A10-Toyopearl resin by purifying AAV2 from a clarified HEK293 cell culture lysate. The two feedstocks utilized in this study – namely a HEK293 cell lysate featuring an AAV2 titer ~$1.9 \cdot 10^{12}$ vp/mL and a HCP titer ~0.3 mg/mL, and a Sf9 cell lysate containing AAV2 at ~$1.56 \cdot 10^{12}$ vp/mL and HCPs at ~1.1 mg/mL – are representative of bioreactor harvests in the gene therapy industry; similarly, a residence time (RT) of 3 mins for both binding and washing steps was adopted based on industrial operating conditions. The chromatograms of AAV2 purification are presented in **Figure S3**, while the analysis of the collected fractions via size exclusion (SEC) and steric exclusion chromatography (SXC) are reported in **Figures S4** and **S5**. Finally, the resulting values of AAV2 yield and logarithmic removal of HEK293 host cell proteins (HCP LRV) from the HEK293 and Sf9 feedstocks are summarized in **Figure 3A** and **3B** respectively.

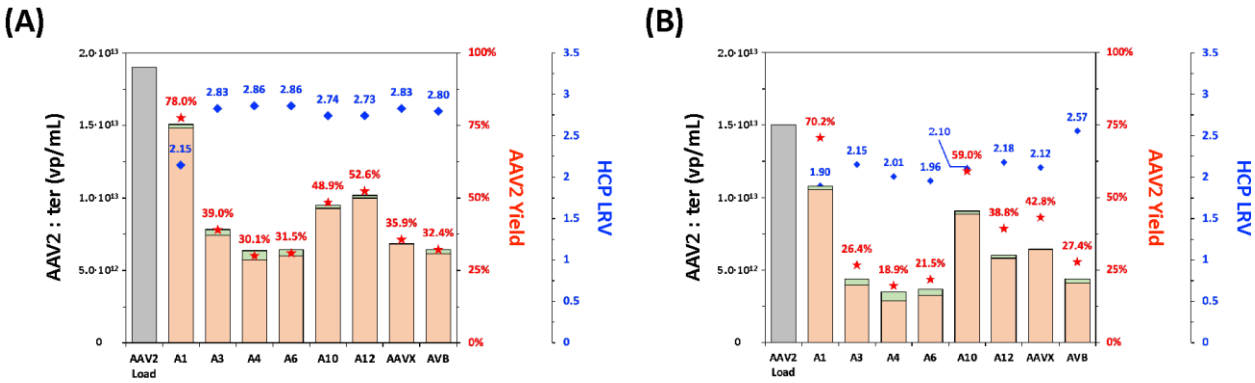


***Figure 3.*** *Values of loss (orange, calculated as the ratio of the AAV titer in the flow-through and wash fractions vs. load) and yield (green, calculated as the ratio of the AAV titer in the elution fraction vs. load) of AAV2 and logarithmic reduction of HCPs (HCP LRV, red triangles) obtained via chromatographic purification of AAV2 from* ***(A)*** *a clarified HEK293 cell lysate (AAV2 titer: ~1.9·10$^{12}$ vp/mL; HCP titer: ~0.3 mg/mL) and* ***(B)*** *a clarified Sf9 cell lysate (AAV2 titer: ~1.56·10$^{12}$ vp/mL; HCP titer: ~1.1 mg/mL) using adsorbents (A1) CYIHFSGYTNYNPSLKS-, (A4) CYGHFSGYGNYGPC-, and (A10) CVIDGSQSTDDDKIC-Toyopearl resins together with control adsorbents POROS™ CaptureSelect™ AAVX (AAVX) and AVB Sepharose HP (AVB) resins. The AAV titer in the flow-through, wash, and elution fractions was measured using serotype-specific ELISA kits.*

The results of AAV2 purification from the HEK293 cell lysate (**Figure 3A**) mirror the corresponding values obtained in non-competitive conditions in **Figure 2B**: *(i)* little-to-no product loss was observed in the flow-through and wash fractions, confirming that the peptides maintain a strong AAV biorecognition when loaded with complex feedstocks; *(ii)* the product yields, ranging between 30% (A4- and A6-Toyopearl resins) and 78% (A1-Toyopearl resins), were either on par with or substantially higher than those returned by the reference POROS™ CaptureSelect™ AAVX Affinity and AVB Sepharose HP resins; and *(iii)* the values of HCP LRV were consistently above 2, reaching values as high as 2.86, corresponding to a > 720-fold decrease of protein contaminants, thus matching the reference adsorbents in terms of product purity as well. The analysis of the feedstock and elution fractions via size exclusion chromatography (SEC, **Figure S4**) and steric exclusion chromatography (SXC, **Figure S5**) offer an at-a-glance of the AAV2 purification performance of the selected resins. While HEK293 ELISA assays returns the titer of HCPs only, analytical chromatography provides a quantitative measure of all process-related impurities – including denatured or hydrolyzed HCPs, other non-proteinaceous metabolites, host cell DNA and RNA, media components – as well as product-related impurities – such as capsid fragments. Mirroring the ELISA results, the SEC and SXC results demonstrate the high purity of the AAV2 eluted from the peptide-based adsorbents. Specifically, the comparative analysis of the SEC chromatograms returns global values of impurity decrease of 150-fold for A1-Toyopearl resin, 730-fold for A4-Toyopearl resin, and 550-fold for A10-Toyopearl resin. Similar results were provided by the SXC chromatograms, confirming that peptide-based adsorbents deliver eluates whose purity is comparable to that afforded by the affinity adsorbents utilized in the gene therapy industry.

Excellent results were also obtained on the front of AAV2 purification from the Sf9 cell lysate (**Figure 3B**). As observed before, A1-Toyopearl resin afforded the highest product yield (70%), although the purity of the eluate was somewhat wanting, whereas A4- and A10-Toyopearl resin performed comparably to the control resins. While we cannot exclude that the association of some HCPs to the AAV2 capsids may be responsible for the lower purity of the A1 eluates (*note:* the titer of HEK293 and Sf9 HCPs in the A1 *vs.* AAVX eluates differ by 9.7 and 13.7μg/mL,

respectively, corresponding to 2.7 and 1.2% of the HCPs in the feedstocks), we can also expect that A1 – as a small peptide ligand – does not quite match the binding selectivity of its $V_HH$ counterparts. This can be alleviated by decreasing its density on the surface of the resin by further optimizing its sequence, which will be the object of future studies. We should also note that, unlike the HEK293 cell lysate, the Sf9 harvest features a significantly higher HCP titer (0.3 *vs.* 1.1 mg/mL, respectively), which motivates why the values of HCP LRV are lower than those reported in **Figure 3A**. Nonetheless, the concentration of residual HCPs in the eluates from the peptide-based adsorbents were consistently below 35 μg/mL, in line with eluates of affinity resins characteristic of chromatographic processes for biotherapeutics.

The purification performance of the peptide-based adsorbents is particularly remarkable when considering that elution is conducted under near-physiological pH. To quantify the benefits of mild elution, we conducted a comparative measurement of the transduction activity on human epithelial cells (HT1080) of the AAV2 isolated from HEK293 cell culture lysate using A1-, A4-, and A10-Toyopearl resins *vs.* POROS™ CaptureSelect™ AAVX resin (*note:* the gene encapsidated in the target AAV2 encodes for green fluorescence protein (GFP), which enables quantifying the transduction activity via fluorescence flow cytometry). The transduction activity – namely, the ability of a virus to effectively deliver its gene payload to the target cells – is a critical quality parameter of viral vectors and is significantly impacted by the process parameters. AAVs, like most viral vectors, are prone to lose their activity in response to variations in buffer conductivity and pH used to control adsorption and elution during chromatographic purification. Current affinity resins, however, require a rather acidic elution pH, in the range ~ 2 - 3 depending upon serotype and desired elution yield (> 50%), to achieve sufficient product yield. By enabling elution under significantly milder conditions (1M $MgCl_2$ in the 20 mM Bis-Tris buffer at pH 6.0), the proposed peptide-based adsorbents are expected to return products with higher transduction activity than their commercial counterparts. The values collated in **Figure 4** confirm this hypothesis, showing that the activity of AAV2 eluted at pH 6 is between 1.5- and 2.2-fold higher than those isolated by the POROS™ AAVX resin. Remarkable is the activity of AAV2 purified by A1- and A10-Toyopearl resins, which, at 59% and 62% transduction relative to the AAV2 in the feedstock, match the values obtained via CsCl and iodixanol gradient ultracentrifugation.[11,52] In this context, we note that the peptide-based resins release mostly intact and gene-loaded AAV2 particles, showing no signs of capsid fragmentation or aggregation (**Figure S6**).

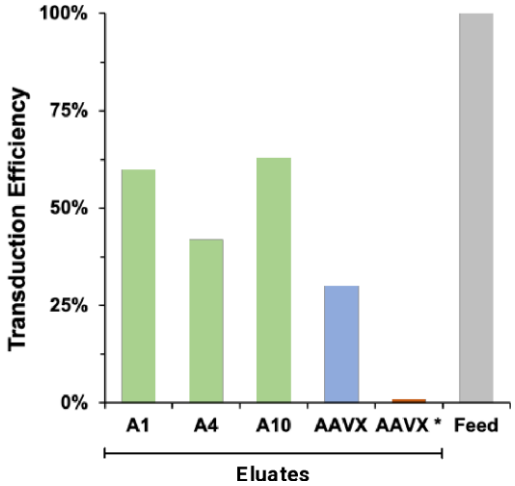


***Figure 4.*** *Values of relative transduction efficiency of AAV2 purified from a clarified HEK293 cell lysate using peptide-based adsorbents (A1) CYIHFSGYTNYNPSLKS-, (A4) CYGHFSGYGNYGPC-, and (A10) CVIDGSQSTDDDKIC-Toyopearl*

*resins together with control adsorbent POROS™ CaptureSelect™ AAVX resin (note: AAVX and AAVX* denote the eluate that was neutralized respectively immediately and 48 hrs after collection). The transduction efficiency (TU/vp) of eluted AAV2 was measured on human epithelial (HT1080; $10^7$ vp per cell) by performing a green fluorescence assay using a CytoFLEX Flow Cytometer. The values of relative transduction efficiency were calculated as the ratio of transduction efficiency of eluted AAV2 vs. AAV2 in the feedstock.*

### 3.4. Dynamic AAV binding capacity and reusability of peptide-based adsorbents in competitive mode

Two additional performance parameters, which – together with the values of yield, purity, and activity of the recovered AAVs – determine the suitability of an affinity resin for industrial biopharmaceutical manufacturing are the dynamic binding capacity at 10% product breakthrough ($DBC_{10\%}$) and the reusability upon subsequent cleaning in place. Accordingly, we measured the $DBC_{10\%}$ of (A1) CYIHFSGYTNYNPSLKS-, (A4) CYGHFSGYGNYGPC-, and (A10) CVIDGSQSTDDDKIC-Toyopearl resins via frontal loading of a clarified lysate containing AAV2 at the titer of $2.51 \cdot 10^{12}$ vp/mL at the residence time (RT) of 3 min (*note:* the clarified lysate was adopted in lieu of a pure AAV2 solution to provide a realistic evaluation of the binding capacity of the resins, whose operation is intended for competitive conditions; the adopted RT is recommended for POROS™ AAVX and AVB Sepharose resins and was therefore adopted to ensure comparability).[64,65] The values of $DBC_{10\%}$, compared in **Table 3**, demonstrate that the peptide-based adsorbents, notwithstanding the milder binding strength, feature an AAV binding capacity on par with or exceeding that of commercial affinity resins. This can be ascribed to the multi-site interaction governing the AAV adsorption by the peptide-functionalized surface, whose binding strength effectively matches that of protein-functionalized adsorbents. This decouples the value of binding capacity from the single AAV:peptide binding strength and makes it mostly – or solely – dependent on the specific surface of the resin.

Secondly, the binding capacity and selectivity of an affinity resin can decrease over time due to several factors, such as chemical degradation, physical damage, and fouling, leading to a loss of product yield and purity as well as additional costs related to the replacement and validation of the adsorbent. Unlike Protein A-based resins for antibody purification, whose lifetime has now reached 150 – 200 cycles with intermediate caustic cleaning in place, the commercial affinity resins for AAV purification cannot withstand harsh alkaline treatment and rapidly lose their binding capacity, mandating frequent column replacement. We therefore evaluated the reusability of the peptide-based adsorbents to withstand 20 cycles of AAV2 purification followed by regeneration and cleaning in place. As shown in **Table 3**, A1-, A4, and A10-Toyopearl resins consistently maintained their $DBC_{10\%}$ (~ 10% variation), demonstrating the chemical stability of the selected peptides and their linkage to the resin.

***Table 3.*** *Values of dynamic AAV2 binding capacity ($DBC_{10\%}$) of peptide-functionalized resins loaded (RT: 3 min) with a clarified HEK293 cell lysate containing AAV2 at the titer of $2.51 \cdot 10^{12}$ vp/mL. - -: not available.*

| Resin | $DBC_{10\%}$ (vp AAV per mL of resin) | |
|---|---|---|
| | Cycle 1 | Cycle 20 |
| A1-Toyopearl | $2.80 \cdot 10^{14}$ | $2.35 \cdot 10^{14}$ |
| A4-Toyopearl | $2.52 \cdot 10^{14}$ | $2.16 \cdot 10^{14}$ |
| A10 -Toyopearl | $2.10 \cdot 10^{14}$ | $2.01 \cdot 10^{14}$ |
| POROS™ AAVX | $5.60 \cdot 10^{14}$ | - - |

## 4. Conclusions

Viral vectors are rapidly becoming – and will soon be – an integral part of modern medicine: as the discourse on biomanufacturing evolves (*e.g.*, the layout of platform processes, whether scaling-up *vs.* scaling-out will meet the growing demand, or the standardization and comparability in the process analytical technology, etc.), the need of a portfolio of bioprocess technologies dedicated to the expression, purification, and analytical characterization of viral vectors becomes every day more evident. Contributing to the efforts on improving downstream technologies, this study presents an ensemble of small peptide affinity ligands designed to transform AAV purification as they provide *(i)* selective as well as flexible product capture, being serotype-agnostic and applicable to both HEK293 and Sf9 fluids; *(ii)* gentle elution, allowing product release under near-physiological pH; and *(iii)* robust reusability, maintaining a high binding capacity over multiple purification cycles. Furthermore, unlike affinity adsorbents that rely on antibody-derived ligands, the proposed adsorbents are undoubtedly more scalable and affordable, and they leverage the ability to mass manufacture GMP-quality peptides at relatively low cost (~US$8 per gram per amino acid residue, when manufactured at > 10 kg scale per year).[53,54] Combining the cost of synthesis with the average values of number of residues (~15-17) and molecular weight (~1.5-1.7 kg per mol) of the peptide ligands, their density on the resin surface (~0.03 mol per liter), and the cost of the base resin (~$2,500 per liter) indicates that direct material cost of the peptide-functionalized adsorbent ranges between $7,900 and $9,500 per liter, when produced at the ~100 liters scale (*note:* direct labor and manufacturing overhead are not factored). These considerations, combined with the purification performance of peptide-functionalized adsorbents presented by our team and by several others in the literature,[9,11,55-63] show the promise of this technology to transform the biomanufacturing of modern medicines and reduce their cost (*note:* the latter is of particular concern, given the price tag of gene therapies well above US$1M per patient). Under the light of these considerations, our team plans to *(i)* demonstrate further the technology introduced in this study by purifying AAVs of different serotypes from a variety of HEK293 and Sf9 fluids; and *(ii)* leverage the *in silico-in vitro* toolbox for ligand development to establish a portfolio of peptide-based purification tools for the other key viral vector families, namely lentivirus (LV), adenovirus (Ad), and baculovirus (BV).

**Acknowledgements.** The authors wish to acknowledge the funding provided by the National Science Foundation (CBET 1743404 and CBET 1653590), the Novo Foundation (AIM-Bio Grant NNF19SA0035474) as well as the generous support of the Golden LEAF Biomanufacturing Training and Education Center (BTEC) and the North Carolina Viral Vector Initiative in Research and Learning (NC-VVIRAL) at NC State University.

**Author Contributions.** S.S., W.C., E.B., P.G.-C., W.K.S., C.C., and A.M. conducted the experimental work. J.P., G.G., K.R., M.A.D., and S.M. conceived the work and wrote the manuscript.

**Data Availability Statement.** The data that support the findings of this study are available from the corresponding author, S.M., upon request.

**Conflict of interest.** The authors declare no conflict of interest.

**References**


(1) Bulcha, J. T.; Wang, Y.; Ma, H.; Tai, P. W. L.; Gao, G. Viral Vector Platforms within the Gene Therapy Landscape. *Signal Transduct. Target. Ther.* **2021**, *6* (1), 53. https://doi.org/10.1038/s41392-021-00487-6.

(2) Fukuhara, H.; Ino, Y.; Todo, T. Oncolytic Virus Therapy: A New Era of Cancer Treatment at Dawn. *Cancer Sci.* **2016**, *107* (10), 1373–1379. https://doi.org/10.1111/cas.13027.

(3) Rodrigues, A. F.; Soares, H. R.; Guerreiro, M. R.; Alves, P. M.; Coroadinha, A. S. Viral Vaccines and Their Manufacturing Cell Substrates: New Trends and Designs in Modern Vaccinology. *Biotechnol. J.* **2015**, *10* (9), 1329–1344. https://doi.org/10.1002/biot.201400387.

(4) Zaidi, S. S.-A.; Mansoor, S. Viral Vectors for Plant Genome Engineering. *Front. Plant Sci.* **2017**, *8*.

(5) Chandler, R. J.; Sands, M. S.; Venditti, C. P. Recombinant Adeno-Associated Viral Integration and Genotoxicity: Insights from Animal Models. *Hum. Gene Ther.* **2017**, *28* (4), 314–322. https://doi.org/10.1089/hum.2017.009.

(6) Verdera, H. C.; Kuranda, K.; Mingozzi, F. AAV Vector Immunogenicity in Humans: A Long Journey to Successful Gene Transfer. *Mol. Ther.* **2020**, *28* (3), 723–746. https://doi.org/10.1016/j.ymthe.2019.12.010.

(7) Ura, T.; Okuda, K.; Shimada, M. Developments in Viral Vector-Based Vaccines. *Vaccines* **2014**, *2* (3), 624–641. https://doi.org/10.3390/vaccines2030624.

(8) Terova, O.; Soltys, S.; Hermans, P.; de Rooij, J.; Detmers, F. Overcoming Downstream Purification Challenges for Viral Vector Manufacturing: Enabling Advancement of Gene Therapies in the Clinic. *Cell Gene Ther. Insights* **2018**, *4*, 101–111. https://doi.org/10.18609/cgti.2018.017.

(9) Chu, W.; Shastry, S.; Barbieri, E.; Prodromou, R.; Greback-Clarke, P.; Smith, W.; Moore, B.; Kilgore, R.; Cummings, C.; Pancorbo, J.; Gilleskie, G.; Daniele, M. A.; Menegatti, S. Peptide Ligands for the Affinity Purification of Adeno-Associated Viruses from HEK293 Cell Lysates. *bioRxiv* **2023**, 2023.02.19.529155. https://doi.org/10.1101/2023.02.19.529155.

(10) Łącki, K. M.; Riske, F. J. Affinity Chromatography: An Enabling Technology for Large-Scale Bioprocessing. *Biotechnol. J.* **2020**, *15* (1), 1800397. https://doi.org/10.1002/biot.201800397.

(11) Florea, M.; Nicolaou, F.; Pacouret, S.; Zinn, E. M.; Sanmiguel, J.; Andres-Mateos, E.; Unzu, C.; Wagers, A. J.; Vandenberghe, L. H. High-Efficiency Purification of Divergent AAV Serotypes Using AAVX Affinity Chromatography. *Mol. Ther. - Methods Clin. Dev.* **2023**, *28*, 146–159. https://doi.org/10.1016/j.omtm.2022.12.009.

(12) Adams, B.; Bak, H.; Tustian, A. D. Moving from the Bench towards a Large Scale, Industrial Platform Process for Adeno-Associated Viral Vector Purification. *Biotechnol. Bioeng.* **2020**, *117* (10), 3199–3211. https://doi.org/10.1002/bit.27472.

(13) Kilgore, R.; Chu, W.; Bhandari, D.; Fischler, D.; Carbonell, R. G.; Crapanzano, M.; Menegatti, S. Development of Peptide Affinity Ligands for the Purification of Polyclonal and Monoclonal Fabs from Recombinant Fluids. *J. Chromatogr. A* **2023**, *1687*, 463701. https://doi.org/10.1016/j.chroma.2022.463701.

(14) Xiao, X.; Kilgore, R.; Sarma, S.; Chu, W.; Menegatti, S.; Hall, C. K. De Novo Discovery of Peptide-Based Affinity Ligands for the Fab Fragment of Human Immunoglobulin G. *J. Chromatogr. A* **2022**, *1669*, 462941. https://doi.org/10.1016/j.chroma.2022.462941.

(15) Chu, W.; Sripada, S. A.; Reese, H. R.; Bhandari, D.; Adams, A.; Sly, J.; Crapanzano, M.; Menegatti, S. Purification of Polyclonal Immunoglobulin G from Human Serum Using Peptide-Based Adsorbents. *AIChE J.* **2021**, *67* (12), e17482. https://doi.org/10.1002/aic.17482.
(16) Chu, W.; Prodromou, R.; Day, K. N.; Schneible, J. D.; Bacon, K. B.; Bowen, J. D.; Kilgore, R. E.; Catella, C. M.; Moore, B. D.; Mabe, M. D.; Alashoor, K.; Xu, Y.; Xiao, Y.; Menegatti, S. Peptides and Pseudopeptide Ligands: A Powerful Toolbox for the Affinity Purification of Current and next-Generation Biotherapeutics. *J. Chromatogr. A* **2021**, *1635*, 461632. https://doi.org/10.1016/j.chroma.2020.461632.
(17) Chu, W.; Prodromou, R.; Moore, B.; Elhanafi, D.; Kilgore, R.; Shastry, S.; Menegatti, S. Development of Peptide Ligands for the Purification of α-1 Antitrypsin from Cell Culture Fluids. *J. Chromatogr. A* **2022**, *1679*, 463363. https://doi.org/10.1016/j.chroma.2022.463363.
(18) Prodromou, R.; Moore, B. D.; Chu, W.; Deal, H.; San Miguel, A.; Brown, A. C.; Daniele, M. A.-A.; Pozdin, V. A.; Menegatti, S. Molecular Engineering of Cyclic Azobenzene-Peptide Hybrid Ligands for the Purification of Human Blood Factor VIII via Photo-Affinity Chromatography. *Adv. Funct. Mater.* **2023**, *n/a* (n/a), 2213881. https://doi.org/10.1002/adfm.202213881.
(19) Prodromou, R.; Day, K. N.; Saberi-Bosari, S.; Schneible, J. D.; Mabe, M. D.; San Miguel, A.; Daniele, M. A.; Pozdin, V.; Menegatti, S. Engineering Next Generation Cyclized Peptide Ligands for Light-Controlled Capture and Release of Therapeutic Proteins. *Adv. Funct. Mater.* **2021**, *31* (27), 2101410. https://doi.org/10.1002/adfm.202101410.
(20) Brennan, T. A.; Wilson, J. M. The Special Case of Gene Therapy Pricing. *Nat. Biotechnol.* **2014**, *32* (9), 874–876. https://doi.org/10.1038/nbt.3003.
(21) Hanwell, M. D.; Curtis, D. E.; Lonie, D. C.; Vandermeersch, T.; Zurek, E.; Hutchison, G. R. Avogadro: An Advanced Semantic Chemical Editor, Visualization, and Analysis Platform. *J. Cheminformatics* **2012**, *4* (1), 17. https://doi.org/10.1186/1758-2946-4-17.
(22) Schmid, N.; Eichenberger, A. P.; Choutko, A.; Riniker, S.; Winger, M.; Mark, A. E.; van Gunsteren, W. F. Definition and Testing of the GROMOS Force-Field Versions 54A7 and 54B7. *Eur. Biophys. J.* **2011**, *40* (7), 843–856. https://doi.org/10.1007/s00249-011-0700-9.
(23) Ke, Q.; Gong, X.; Liao, S.; Duan, C.; Li, L. Effects of Thermostats/Barostats on Physical Properties of Liquids by Molecular Dynamics Simulations. *J. Mol. Liq.* **2022**, *365*, 120116. https://doi.org/10.1016/j.molliq.2022.120116.
(24) Singhal, A.; Schneible, J. D.; Lilova, R. L.; Hall, C. K.; Menegatti, S.; Grafmüller, A. A Multiscale Coarse-Grained Model to Predict the Molecular Architecture and Drug Transport Properties of Modified Chitosan Hydrogels. *Soft Matter* **2020**, *16* (47), 10591–10610. https://doi.org/10.1039/D0SM01243B.
(25) Schneible, J. D.; Shi, K.; Young, A. T.; Ramesh, S.; He, N.; Dowdey, C. E.; Dubnansky, J. M.; Lilova, R. L.; Gao, W.; Santiso, E.; Daniele, M.; Menegatti, S. Modified Gaphene Oxide (GO) Particles in Peptide Hydrogels: A Hybrid System Enabling Scheduled Delivery of Synergistic Combinations of Chemotherapeutics. *J. Mater. Chem. B* **2020**, *8* (17), 3852–3868. https://doi.org/10.1039/D0TB00064G.
(26) Schneible, J. D.; Singhal, A.; Lilova, R. L.; Hall, C. K.; Grafmüller, A.; Menegatti, S. Tailoring the Chemical Modification of Chitosan Hydrogels to Fine-Tune the Release of a Synergistic Combination of Chemotherapeutics. *Biomacromolecules* **2019**, *20* (8), 3126–3141. https://doi.org/10.1021/acs.biomac.9b00707.

(27) Madhavi Sastry, G.; Adzhigirey, M.; Day, T.; Annabhimoju, R.; Sherman, W. Protein and Ligand Preparation: Parameters, Protocols, and Influence on Virtual Screening Enrichments. *J. Comput. Aided Mol. Des.* **2013**, *27* (3), 221–234. https://doi.org/10.1007/s10822-013-9644-8.

(28) Bas, D. C.; Rogers, D. M.; Jensen, J. H. Very Fast Prediction and Rationalization of PKa Values for Protein–Ligand Complexes. *Proteins Struct. Funct. Bioinforma.* **2008**, *73* (3), 765–783. https://doi.org/10.1002/prot.22102.

(29) Honorato, R. V.; Koukos, P. I.; Jiménez-García, B.; Tsaregorodtsev, A.; Verlato, M.; Giachetti, A.; Rosato, A.; Bonvin, A. M. J. J. Structural Biology in the Clouds: The WeNMR-EOSC Ecosystem. *Front. Mol. Biosci.* **2021**, *8*.

(30) van Zundert, G. C. P.; Rodrigues, J. P. G. L. M.; Trellet, M.; Schmitz, C.; Kastritis, P. L.; Karaca, E.; Melquiond, A. S. J.; van Dijk, M.; de Vries, S. J.; Bonvin, A. M. J. J. The HADDOCK2.2 Web Server: User-Friendly Integrative Modeling of Biomolecular Complexes. *Comput. Resour. Mol. Biol.* **2016**, *428* (4), 720–725. https://doi.org/10.1016/j.jmb.2015.09.014.

(31) Spiliotopoulos, D.; Kastritis, P. L.; Melquiond, A. S. J.; Bonvin, A. M. J. J.; Musco, G.; Rocchia, W.; Spitaleri, A. DMM-PBSA: A New HADDOCK Scoring Function for Protein-Peptide Docking. *Front. Mol. Biosci.* **2016**, *3*.

(32) Pillay Sirika; Zou Wei; Cheng Fang; Puschnik Andreas S.; Meyer Nancy L.; Ganaie Safder S.; Deng Xuefeng; Wosen Jonathan E.; Davulcu Omar; Yan Ziying; Engelhardt John F.; Brown Kevin E.; Chapman Michael S.; Qiu Jianming; Carette Jan E. Adeno-Associated Virus (AAV) Serotypes Have Distinctive Interactions with Domains of the Cellular AAV Receptor. *J. Virol.* **2017**, *91* (18), e00391-17. https://doi.org/10.1128/JVI.00391-17.

(33) Meyer, N. L.; Chapman, M. S. Adeno-Associated Virus (AAV) Cell Entry: Structural Insights. *Trends Microbiol.* **2022**, *30* (5), 432–451. https://doi.org/10.1016/j.tim.2021.09.005.

(34) Summerford, C.; Bartlett, J. S.; Samulski, R. J. AVβ5 Integrin: A Co-Receptor for Adeno-Associated Virus Type 2 Infection. *Nat. Med.* **1999**, *5* (1), 78–82. https://doi.org/10.1038/4768.

(35) Qing, K.; Mah, C.; Hansen, J.; Zhou, S.; Dwarki, V.; Srivastava, A. Human Fibroblast Growth Factor Receptor 1 Is a Co-Receptor for Infection by Adeno-Associated Virus 2. *Nat. Med.* **1999**, *5* (1), 71–77. https://doi.org/10.1038/4758.

(36) Asokan Aravind; Hamra Julie B.; Govindasamy Lakshmanan; Agbandje-McKenna Mavis; Samulski Richard J. Adeno-Associated Virus Type 2 Contains an Integrin A5β1 Binding Domain Essential for Viral Cell Entry. *J. Virol.* **2006**, *80* (18), 8961–8969. https://doi.org/10.1128/JVI.00843-06.

(37) Akache Bassel; Grimm Dirk; Pandey Kusum; Yant Stephen R.; Xu Hui; Kay Mark A. The 37/67-Kilodalton Laminin Receptor Is a Receptor for Adeno-Associated Virus Serotypes 8, 2, 3, and 9. *J. Virol.* **2006**, *80* (19), 9831–9836. https://doi.org/10.1128/JVI.00878-06.

(38) Blackburn, S. D.; Steadman, R. A.; Johnson, F. B. Attachment of Adeno-Associated Virus Type 3H to Fibroblast Growth Factor Receptor 1. *Arch. Virol.* **2006**, *151* (3), 617–623. https://doi.org/10.1007/s00705-005-0650-6.

(39) Ling, C.; Lu, Y.; Kalsi, J. K.; Jayandharan, G. R.; Li, B.; Ma, W.; Cheng, B.; Gee, S. W. Y.; McGoogan, K. E.; Govindasamy, L.; Zhong, L.; Agbandje-McKenna, M.; Srivastava, A. Human Hepatocyte Growth Factor Receptor Is a Cellular Coreceptor for Adeno-Associated

Virus Serotype 3. *Hum. Gene Ther.* **2010**, *21* (12), 1741–1747. https://doi.org/10.1089/hum.2010.075.
(40) Pasquale, G. D.; Davidson, B. L.; Stein, C. S.; Martins, I.; Scudiero, D.; Monks, A.; Chiorini, J. A. Identification of PDGFR as a Receptor for AAV-5 Transduction. *Nat. Med.* **2003**, *9* (10), 1306–1312. https://doi.org/10.1038/nm929.
(41) Day, K.; Prodromou, R.; Saberi Bosari, S.; Lavoie, A.; Omary, M.; Market, C.; San Miguel, A.; Menegatti, S. Discovery and Evaluation of Peptide Ligands for Selective Adsorption and Release of Cas9 Nuclease on Solid Substrates. *Bioconjug. Chem.* **2019**, *30* (12), 3057–3068. https://doi.org/10.1021/acs.bioconjchem.9b00703.
(42) Barozzi, A.; Lavoie, R. A.; Day, K. N.; Prodromou, R.; Menegatti, S. Affibody-Binding Ligands. *Int. J. Mol. Sci.* **2020**, *21* (11). https://doi.org/10.3390/ijms21113769.
(43) Bowen, J.; Schneible, J.; Bacon, K.; Labar, C.; Menegatti, S.; Rao, B. M. Screening of Yeast Display Libraries of Enzymatically Treated Peptides to Discover Macrocyclic Peptide Ligands. *Int. J. Mol. Sci.* **2021**, *22* (4). https://doi.org/10.3390/ijms22041634.
(44) Bacon, K.; Bowen, J.; Reese, H.; Rao, B. M.; Menegatti, S. Use of Target-Displaying Magnetized Yeast in Screening MRNA-Display Peptide Libraries to Identify Ligands. *ACS Comb. Sci.* **2020**, *22* (12), 738–744. https://doi.org/10.1021/acscombsci.0c00171.
(45) Reese, H. R.; Xiao, X.; Shanahan, C. C.; Chu, W.; Van Den Driessche, G. A.; Fourches, D.; Carbonell, R. G.; Hall, C. K.; Menegatti, S. Novel Peptide Ligands for Antibody Purification Provide Superior Clearance of Host Cell Protein Impurities. *J. Chromatogr. A* **2020**, *1625*, 461237. https://doi.org/10.1016/j.chroma.2020.461237.
(46) Day, K.; Schneible, J. D.; Young, A. T.; Pozdin, V. A.; Van Den Driessche, G.; Gaffney, L. A.; Prodromou, R.; Freytes, D. O.; Fourches, D.; Daniele, M.; Menegatti, S. Photoinduced Reconfiguration to Control the Protein-Binding Affinity of Azobenzene-Cyclized Peptides. *J. Mater. Chem. B* **2020**, *8* (33), 7413–7427. https://doi.org/10.1039/D0TB01189D.
(47) Saberi-Bosari, S.; Omary, M.; Lavoie, A.; Prodromou, R.; Day, K.; Menegatti, S.; San-Miguel, A. Affordable Microfluidic Bead-Sorting Platform for Automated Selection of Porous Particles Functionalized with Bioactive Compounds. *Sci. Rep.* **2019**, *9* (1), 7210. https://doi.org/10.1038/s41598-019-42869-5.
(48) Gao Guangping; Vandenberghe Luk H.; Alvira Mauricio R.; Lu You; Calcedo Roberto; Zhou Xiangyang; Wilson James M. Clades of Adeno-Associated Viruses Are Widely Disseminated in Human Tissues. *J. Virol.* **2004**, *78* (12), 6381–6388. https://doi.org/10.1128/JVI.78.12.6381-6388.2004.
(49) Mietzsch, M.; Jose, A.; Chipman, P.; Bhattacharya, N.; Daneshparvar, N.; McKenna, R.; Agbandje-McKenna, M. Completion of the AAV Structural Atlas: Serotype Capsid Structures Reveals Clade-Specific Features. *Viruses* **2021**, *13* (1). https://doi.org/10.3390/v13010101.
(50) Wang, D.; Zhong, L.; Nahid, M. A.; Gao, G. The Potential of Adeno-Associated Viral Vectors for Gene Delivery to Muscle Tissue. *Expert Opin. Drug Deliv.* **2014**, *11* (3), 345–364. https://doi.org/10.1517/17425247.2014.871258.
(51) Hocquemiller, M.; Giersch, L.; Audrain, M.; Parker, S.; Cartier, N. Adeno-Associated Virus-Based Gene Therapy for CNS Diseases. *Hum. Gene Ther.* **2016**, *27* (7), 478–496. https://doi.org/10.1089/hum.2016.087.
(52) Blessing, D.; Vachey, G.; Pythoud, C.; Rey, M.; Padrun, V.; Wurm, F. M.; Schneider, B. L.; Déglon, N. Scalable Production of AAV Vectors in Orbitally Shaken HEK293 Cells. *Mol. Ther. - Methods Clin. Dev.* **2019**, *13*, 14–26. https://doi.org/10.1016/j.omtm.2018.11.004.

(53) Glaser, V. Reducing the Cost of Peptide Synthesis. *Genet. Eng. Biotechnol. News* **2013**, *33* (13), 32–34. https://doi.org/10.1089/gen.33.13.18.
(54) Bray, B. L. Large-Scale Manufacture of Peptide Therapeutics by Chemical Synthesis. *Nat. Rev. Drug Discov.* **2003**, *2* (7), 587–593. https://doi.org/10.1038/nrd1133.
(55) Nass, S. A.; Mattingly, M. A.; Woodcock, D. A.; Burnham, B. L.; Ardinger, J. A.; Osmond, S. E.; Frederick, A. M.; Scaria, A.; Cheng, S. H.; O'Riordan, C. R. Universal Method for the Purification of Recombinant AAV Vectors of Differing Serotypes. *Mol. Ther. - Methods Clin. Dev.* **2018**, *9*, 33–46. https://doi.org/10.1016/j.omtm.2017.12.004.
(56) Fan, J.; Barbieri, E.; Shastry, S.; Menegatti, S.; Boi, C.; Carbonell, R. G. Purification of Adeno-Associated Virus (AAV) Serotype 2 from Spodoptera Frugiperda (Sf9) Lysate by Chromatographic Nonwoven Membranes. *Membranes* **2022**, *12* (10). https://doi.org/10.3390/membranes12100944.
(57) Overton, L.; Boi, C.; Shastry, S.; Smith-Moore, C.; Balchunas, J.; Sambandan, D.; Gilleskie, G. Development and Delivery of a Hands-on Short Course in AAV Manufacturing to Support Growing Workforce Needs in Gene Therapy. *Hum. Gene Ther.* **2023**. https://doi.org/10.1089/hum.2022.235.
(58) Smith, R. H.; Levy, J. R.; Kotin, R. M. A Simplified Baculovirus-AAV Expression Vector System Coupled With One-Step Affinity Purification Yields High-Titer RAAV Stocks From Insect Cells. *Mol. Ther.* **2009**, *17* (11), 1888–1896. https://doi.org/10.1038/mt.2009.128.
(59) Joshi, P. R. H.; Bernier, A.; Moço, P. D.; Schrag, J.; Chahal, P. S.; Kamen, A. Development of a Scalable and Robust AEX Method for Enriched RAAV Preparations in Genome-Containing VCs of Serotypes 5, 6, 8, and 9. *Mol. Ther. - Methods Clin. Dev.* **2021**, *21*, 341–356. https://doi.org/10.1016/j.omtm.2021.03.016.
(60) Wang, Q.; Lock, M.; Prongay, A. J.; Alvira, M. R.; Petkov, B.; Wilson, J. M. Identification of an Adeno-Associated Virus Binding Epitope for AVB Sepharose Affinity Resin. *Mol. Ther. - Methods Clin. Dev.* **2015**, *2*, 15040. https://doi.org/10.1038/mtm.2015.40.
(61) Dickerson, R.; Argento, C.; Pieracci, J.; Bakhshayeshi, M. Separating Empty and Full Recombinant Adeno-Associated Virus Particles Using Isocratic Anion Exchange Chromatography. *Biotechnol. J.* **2021**, *16* (1), 2000015. https://doi.org/10.1002/biot.202000015.
(62) Qu, G.; Bahr-Davidson, J.; Prado, J.; Tai, A.; Cataniag, F.; McDonnell, J.; Zhou, J.; Hauck, B.; Luna, J.; Sommer, J. M.; Smith, P.; Zhou, S.; Colosi, P.; High, K. A.; Pierce, G. F.; Wright, J. F. Separation of Adeno-Associated Virus Type 2 Empty Particles from Genome Containing Vectors by Anion-Exchange Column Chromatography. *J. Virol. Methods* **2007**, *140* (1), 183–192. https://doi.org/10.1016/j.jviromet.2006.11.019.
(63) Arunkumar, A.; Singh, N. Ultrafiltration Behavior of Recombinant Adeno Associated Viral Vectors Used in Gene Therapy. *J. Membr. Sci.* **2021**, *620*, 118812. https://doi.org/10.1016/j.memsci.2020.118812.
(64) Cytiva, AVB Sepharose High Performance: https://www.cytivalifesciences.com/en/us/shop/chromatography/resins/affinity-specific-groups/avb-sepharose-high-performance-p-05953.
(65) Scientific™, T. POROS™ CaptureSelect™ AAV Resins: AAV8, AAV9, AAVX. https://www.thermofisher.com/document-connect/document-connect.html?url=https://assets.thermofisher.com/TFS-Assets%2FLSG%2Fmanuals%2F100038399_POROS_CapSel_AAV8_AAV9_Resins_UG.pdf.

(66) Gregorevic, P.; Blankinship, M. J.; Allen, J. M.; Crawford, R. W.; Meuse, L; Miller, D. G.; Russell D. W.; Chamberlain, J. S. Systemic delivery of genes to striated muscles using adeno-associated viral vectors. *Nat Med.* **2004**, *10* (8). 828-834. doi: 10.1038/nm1085.
(67) Velez-Fort M.; Bracey, E.F.; Keshavarzi, S.; Rousseau, C.V.; Cossell, L.; Lenzi S. C.; Strom, M.; Margrie,T. W. A Circuit for Integration of Head- and Visual-Motion Signals in Layer 6 of Mouse Primary Visual Cortex. *Neuron.* **2018**, *98* (1). 179-191. doi: 10.1016/j.neuron.2018.02.023.